

Final Report for AOARD Grant 104036 “High Sensitivity Conjugated Polymer/nanoparticle Nanocomposite for Infrared Sensor Applications”

2011.03.03

Name of Principal Investigators: Professor Kung-Hwa Wei

- e-mail address : khwei@mail.nctu.edu.tw
- Institution : Dept. of Materials Science, National Chiao Tung University, Taiwan
- Mailing Address : 1001 University Road, Hsinchu, Taiwan 30049
- Phone : 886-35-731-871
- Fax : 886-35-724-727

Period of Performance: 02/01/2007 – 01/31/2011

Part I. An Organic Hole Transport Layer Enhances the Performance of Colloidal PbSe Quantum Dot Photovoltaic Devices

Abstract: A thin poly(3,4-ethylenedioxythiophene):poly(styrene sulfonate) (PEDOT:PSS) hole transport layer enhances the AM1.5 power conversion efficiency of a PbSe quantum dot (QD)-containing photovoltaic device to 2.4%, from 1.5% for a standard PbSe QD device, a relative increase of 60%. Synchrotron X-ray reflectivity measurements revealed that the roughness of the interfaces between the various layers decreased dramatically in the presence of the PEDOT:PSS layer. In addition, the device life time under continuous simulated AM1.5 irradiation (100 mW cm⁻²), measured in terms of the time required to reach 80% of the normalized efficiency, for the PbSe QD device incorporating the PEDOT:PSS hole transport layer was six times longer than that of the standard PbSe QD device.

Introduction:

Fabricating photovoltaic devices using solution-processed materials has many potential benefits, particularly for the rapid and economical preparation of flexible, large-area devices. Solution-processing of organic polymers,^[1,2] inorganic semiconductors,^[3-5] and organic/inorganic hybrids^[6-9] has been adopted widely. One example of the use of conjugated polymers is in the preparation of heterojunction photovoltaic devices, which have achieved solar conversion efficiencies greater than 7%.^[10] Nevertheless, because composites of low-bandgap conjugated polymers and fullerene derivatives remain active only at wavelengths from 300 to 800 nm, they fail to harvest most of the radiation in the infrared (IR) spectral region. By virtue of the quantum size effect, colloidal quantum dots (QDs) of Pb salts have absorption characteristics that can be tuned throughout the IR spectrum.^[11-13] Furthermore, colloidal Pb-salt QDs can potentially undergo multiple exciton generation,^[14,15] the generation of more than one electron/hole pair. If multiexciton formation, dissociation, and charge collection were all efficient events, the resulting enhanced photocurrent would lead to an increase in the solar energy conversion efficiency.^[16] Hence, the development of Pb-salt colloidal QDs for use in optoelectronic devices has emerged recently as an active area of investigation.^[17-20]

Using a layer-by-layer (LBL) technique—one that involves alternate (i) dip-coating or spin-coating of QDs onto a patterned indium tin oxide (ITO) substrate and (ii) exposing the QD films to a bidentate ligand to can effectively remove the long, insulating oleate ligands from the as-synthesized PbSe QDs—has resulted in increased conductivities of PbSe QD films and excellent photovoltaic performance.^[4,5,21] The first example of the use of LBL processing of PbSe QDs to form a double-layer device structure led to an AM1.5 power conversion efficiency (PCE) of 1.1%.^[22] Later, it was demonstrated that PbSe QD photovoltaic devices exhibit superior performance, with AM1.5 PCEs of ca. 2.1%.^[23] Subsequently, large improvements in the open-circuit voltages (Voc) were obtained when combining PbSxSe1-x QDs^[24] or PbSe QD/ZnO heterojunctions^[25,26] with the LBL technique, resulting in higher PCEs.

Because a completed QD active layer can take more than 20 cycles of solution processing steps using the LBL technique, the quality of the interfaces between the active layer and the electrodes, which is sensitively dependent on the substrate electrode surface, is critical for good charge transport to occur

Report Documentation Page

Form Approved
OMB No. 0704-0188

Public reporting burden for the collection of information is estimated to average 1 hour per response, including the time for reviewing instructions, searching existing data sources, gathering and maintaining the data needed, and completing and reviewing the collection of information. Send comments regarding this burden estimate or any other aspect of this collection of information, including suggestions for reducing this burden, to Washington Headquarters Services, Directorate for Information Operations and Reports, 1215 Jefferson Davis Highway, Suite 1204, Arlington VA 22202-4302. Respondents should be aware that notwithstanding any other provision of law, no person shall be subject to a penalty for failing to comply with a collection of information if it does not display a currently valid OMB control number.

1. REPORT DATE 04 MAR 2011		2. REPORT TYPE FInal		3. DATES COVERED 29-03-2010 to 01-03-2011	
4. TITLE AND SUBTITLE High-Sensitivity Conjugated Polymer/Nanoparticle Nanocomposites for Infrared Sensor Applications IV				5a. CONTRACT NUMBER FA23861014036	
				5b. GRANT NUMBER	
				5c. PROGRAM ELEMENT NUMBER	
6. AUTHOR(S) Kung-Hwa Wei				5d. PROJECT NUMBER	
				5e. TASK NUMBER	
				5f. WORK UNIT NUMBER	
7. PERFORMING ORGANIZATION NAME(S) AND ADDRESS(ES) National Chiao Tung University,1001 Ta Hsueh Rd,Hsinchu 30049,Taiwan,TW,30049				8. PERFORMING ORGANIZATION REPORT NUMBER N/A	
9. SPONSORING/MONITORING AGENCY NAME(S) AND ADDRESS(ES) AOARD, UNIT 45002, APO, AP, 96337-5002				10. SPONSOR/MONITOR'S ACRONYM(S) AOARD	
				11. SPONSOR/MONITOR'S REPORT NUMBER(S) AOARD-104036	
12. DISTRIBUTION/AVAILABILITY STATEMENT Approved for public release; distribution unlimited					
13. SUPPLEMENTARY NOTES					
14. ABSTRACT This is the final report of a research project to improve the electron transport properties of lead selenide quantum dots and cadmium selenide tetrapods.					
15. SUBJECT TERMS Nanocomposites, Polymer composites, Infrared Technology					
16. SECURITY CLASSIFICATION OF:			17. LIMITATION OF ABSTRACT Same as Report (SAR)	18. NUMBER OF PAGES 31	19a. NAME OF RESPONSIBLE PERSON
a. REPORT unclassified	b. ABSTRACT unclassified	c. THIS PAGE unclassified			

across them and to achieve good device performance.^[27] Moreover, the alignment between the valence band of the QDs and the work function of the metal oxide anode will affect the open-circuit voltage of the photovoltaic devices. Hence, a high-quality interface must exist between the anode of the device and the first QD layer. In this study, we introduced a thin (ca. 20 nm) poly(3,4-ethylenedioxythiophene):poly(styrene sulfonate) (PEDOT:PSS) hole transport layer into the interface between a tri-layered PbSe QD active layer and ITO substrate to improve the interfacial smoothness and band alignment and, thereby, enhance the device's photovoltaic performance and life time. The fabrication of these devices is described in the Experimental section; the device structure comprised an ITO anode, Al/Ca cathode, and PbSe QD active layer, with or without a PEDOT:PSS layer.

Results and Discussion:

Figure 1 displays the current density–voltage characteristics of a device incorporating a 95-nm-thick layer of 4.5-nm-diameter PbSe QDs under AM 1.5G conditions (100 mW cm^{-2} , 25°C) and in the dark. The dark current curves of the devices reveal a turn-on voltage of ca. 0.1 V. The PCE for the device incorporating a 20-nm-thick PEDOT:PSS layer was 2.4%, up from 1.5% for the standard device. This increase of 60% in the PCE of the device incorporating the PEDOT:PSS layer, relative to that of the standard device, resulted from increases in the values of both V_{oc} and the short-circuit current density (J_{sc}). The value of V_{oc} of 0.24 V for the device featuring the PEDOT:PSS layer was ca. 33% greater than that of 0.18 V for the standard device. The increase in V_{oc} can be explained in terms of the superior interfacial energy level offset in the device in the presence of the PEDOT:PSS layer than in its absence. Because the incorporated PEDOT:PSS layer has a work function of 5.1 eV, positioned between the valence band of 5.3 eV^[25,28] for the 4.5-nm-diameter PbSe QDs and the work function of 4.8 eV of the ITO electrode, this kind of band energy alignment facilitates the transport of dissociated holes to the anode. The inset of **Figure 1** displays the energy band diagram for the various layers in the device. The value of J_{sc} increased to 21.9 mA cm^{-2} for the device incorporating the PEDOT:PSS layer from 18.0 mA cm^{-2} for the unmodified device, an increase of ca. 20%, presumably because of superior interfacial contacts and, therefore, improved carrier transport between the PbSe QDs and the PEDOT:PSS layer. The fill factors (FFs) of these two devices, however, were similar. **Table 1** lists the current density–voltage characteristics of the PbSe QD device, incorporating a PEDOT:PSS intermediate layer, under 100 mW cm^{-2} solar AM1.5G illumination.

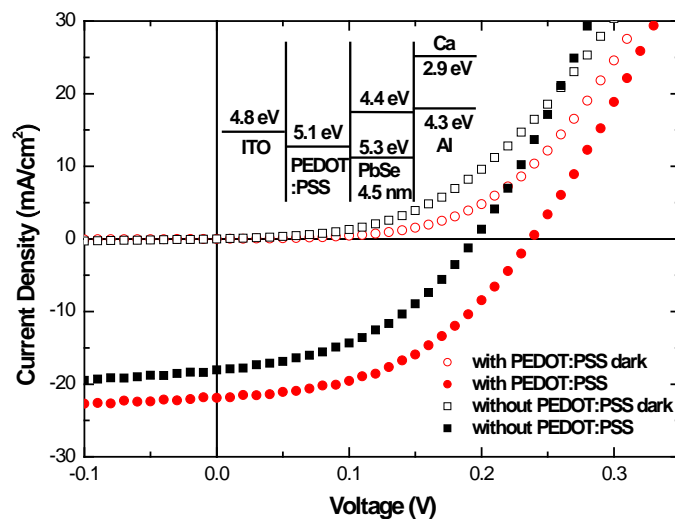


Figure 1. Current density–voltage characteristics of 4.5-nm-diameter PbSe QD devices incorporating a PEDOT:PSS intermediate layer, recorded in the dark and under solar illumination (100 mW cm^{-2}). Inset: Energy-level diagram for a PbSe QD photovoltaic device.

Table 1. Performance parameters of PbSe QD devices incorporating a PEDOT:PSS intermediate layer, under solar illumination.

Device structure	V_{oc}^a (V)	J_{sc}^b (mA cm ⁻²)	FF ^c (%)	η^d (%)
ITO/PbSe/Ca/Al	0.19	18.0	44.0	1.5
ITO/PEDOT:PSS/PbSe/Ca/Al	0.24	21.9	45.5	2.4

^a V_{oc} : Open-circuit voltage. ^b J_{sc} : Short-circuit current density. ^c FF: Fill factor. ^d η : PCE. Solar: AM1.5G (100 mW cm⁻²).

Figure 2a presents a cross-sectional TEM image of a device incorporating a PEDOT:PSS layer (thickness: 20 nm) and a PbSe QD active layer (thickness: 95 ± 5 nm); two interfaces are clearly evident in the active layer (i.e., PbSe-1–PbSe-2 and PbSe-2–PbSe-3). The thickness of this active layer (ca. 95 nm) is close to the optimal value for PbSe QDs devices.^[23–25] Closer examination on the TEM image of the ITO/PEDOT:PSS/PbSe QDs/Ca/Al device structure revealed that the PbSe QDs formed a dense layer that was in intimate physical contact with the PEDOT:PSS layer. The PEDOT:PSS layer apparently provided a smooth transition from the rough ITO surface to the PbSe QD layer. The formation of a smooth active layer, an important feature for efficient device operation, presumably resulted from strong polar interactions between the PbSe QDs and the PEDOT:PSS layer.^[29] Furthermore, the interfacial roughness among the PbSe QD layer, the incorporated PEDOT:PSS layer, and the ITO substrate could be determined quantitatively using synchrotron X-ray reflectivity (XRR) measurements.

Figure 2b presents XRR curves of the PbSe QD films on ITO substrates, in the presence and absence of the PEDOT:PSS layer. The curve of the device incorporating the PEDOT:PSS layer exhibits oscillating behavior between 0.3 and 1.0 nm⁻¹; that of the device lacking a PEDOT:PSS layer appears to be deprived such features, providing further evidence that the presence of the PEDOT:PSS layer results in a reduction of the interfaces' roughness in the device since the physical smoothness of the interface between layers is inversely proportional to the smoothness of its X-ray reflectivity curve. **Table 2** lists the interfacial roughness parameters obtained from curve-fitting the XRR data.^[30] The device prepared without a PEDOT:PSS layer between the ITO substrate and the PbSe layer had a roughness, $\sigma_{ITO/PbSe-1}$, of 2.9 nm. After incorporating a PEDOT:PSS layer on the ITO substrate, the roughness of the interface between the PEDOT:PSS and PbSe QD layers, $\sigma_{PEDOT:PSS/PbSe-1}$, became 1.0 nm, almost a three-fold improvement with respect to that of the original ITO–PbSe QD interface. Furthermore, the fitting results revealed that the PEDOT:PSS layer not only reduced the interfacial roughness of the ITO/PbSe QD substrate but also smoothed the interface between the individually spun PbSe QD layers; the value of $\sigma_{PbSe-1/PbSe-2}$ decreased to 2.8 nm in the presence of PEDOT:PSS layer, from 5.0 nm in its absence.

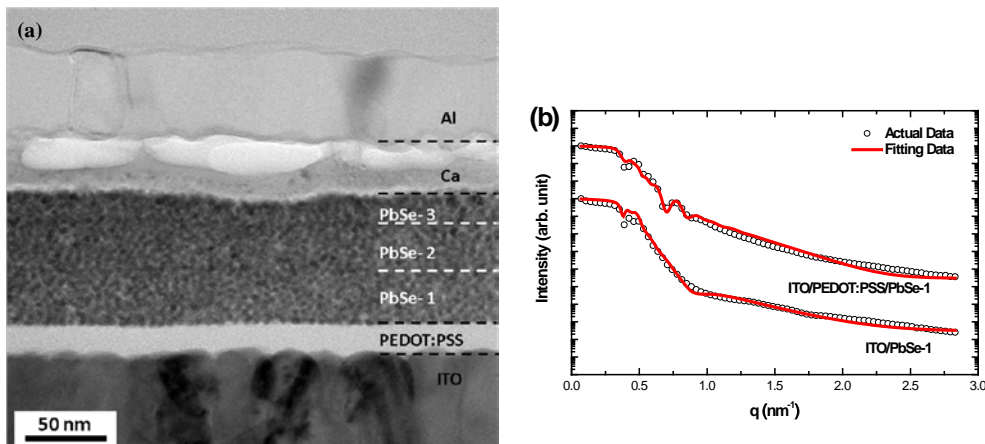


Figure 2. (a) TEM cross-sectional image of the ITO/PEDOT:PSS/PbSe QD film/Ca/Al device stack; scale bar: 50 nm. (b) Synchrotron X-ray reflectance for structures incorporating PbSe QD layers, pre compared with and without a PEDOT:PSS thin layer.

Table 2. Interfacial roughness data obtained by fitting the XRR curves of various layer structures.

ITO/PbSe QDs structure	interfacial roughness nm	ITO/PEDOT:PSS/PbSe QDs structure	interfacial roughness nm
$\sigma_{\text{ITO/PbSe-1}}$	2.9	$\sigma_{\text{ITO/PEDOT:PSS}}$	3.1
–	–	$\sigma_{\text{PEDOT:PSS/PbSe-1}}$	1.0
$\sigma_{\text{PbSe-1/PbSe-2}}$	5.0	$\sigma_{\text{PbSe-1/PbSe-2}}$	2.8

Figure 3a presents current density–voltage plots of PbSe QDs devices featuring various QD sizes in the presence of the PEDOT:PSS layer; **Table 3** lists the photovoltaic properties of these PbSe QD devices. The value of V_{oc} of the device decreases from 0.24 to 0.14 V, while the value of J_{sc} decreased from 21.9 to 17.7 mA cm⁻², upon increasing the size of the PbSe QDs from 4.5 to 6.0 nm. The decrease in V_{oc} upon increasing the QD size was due mainly to the corresponding rising of the valence band and the narrowing of the band gap of the PbSe QDs. **Figure 3b** presents the values of V_{oc} of the devices incorporating different sizes of PbSe QDs plotted with respect to their band gaps (E_g), which we estimated from their sizes as reported in the literature.^[25,28] We observe linear behavior in the plots of V_{oc} against E_g for the devices containing and lacking the PEDOT:PSS layer. For the devices incorporating a PEDOT:PSS layer, the approximately linear behavior between the values of V_{oc} and E_g of the PbSe QDs can be described using the empirical equation

$$V_{oc} = 0.65(E_g / e) - 0.30V \quad (1)$$

where e is the charge of an electron. The slope (0.65) of the line is close to the value reported in the literature for devices containing similar QDs.^[26] The decrease in J_{sc} of the device was caused presumably by increased interfacial roughness when the size of the PbSe QDs increased.

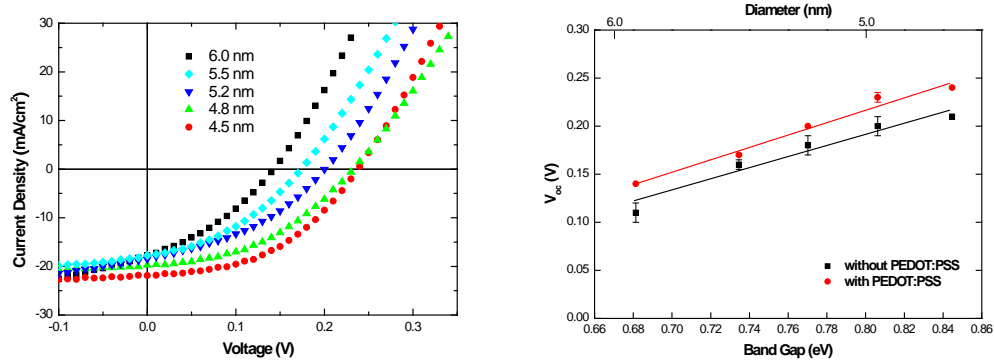


Figure 3. (a) Current density–voltage plots of devices incorporating a PEDOT:PSS layer and PbSe QDs of various average diameters. (b) Open-circuit voltages (V_{oc}) plotted with respect to the diameter of the PbSe QDs and the band gap energy (E_g) of the devices prepared with and without a PEDOT:PSS layer.

Table 3. Performance parameters of devices featuring PbSe QDs of various average diameters and incorporating a PEDOT:PSS intermediate layer, under solar illumination.

PbSe QD size (nm)	V_{oc} (V)	J_{sc} (mA cm ⁻²)	FF (%)	η (%)
6.0	0.14	17.7	34.9	0.86
5.5	0.17	17.8	39.0	1.18
5.2	0.20	18.5	38.2	1.41
4.8	0.23	19.7	43.4	1.97
4.5	0.24	21.9	45.5	2.40

Figure 4 presents external quantum efficiency (EQE) curves for the ITO/PbSe QDs/Ca/Al (standard) and ITO/PEDOT:PSS/PbSe QDs/Ca/Al devices in the wavelength region from 300 to 1800 nm. The device incorporating PEDOT:PSS exhibits a larger EQE than that of the standard device from 360 to 1000 nm, covering the entire visible light range and a small portion of near-IR range. At 650 nm, for instance, the EQE reached 57% for the device containing the PEDOT:PSS layer, compared with 46% for the standard device. The theoretical short-circuit current densities obtained after integrating the EQE curves for the device incorporating PEDOT:PSS and for the standard device were 21.6 and 17.9 mA cm⁻², respectively; these values are close to those (21.9 and 18.0 mA cm⁻², respectively) obtained directly from the *I*-*V* curves, confirming the accuracy of our measurements. **Figure 5** reveals that an approximately linear relationship exists between the short-circuit current density and the incident light intensity over the range from 0 to 100 mW cm⁻², suggesting that this type of device might also find use as a photodetector.

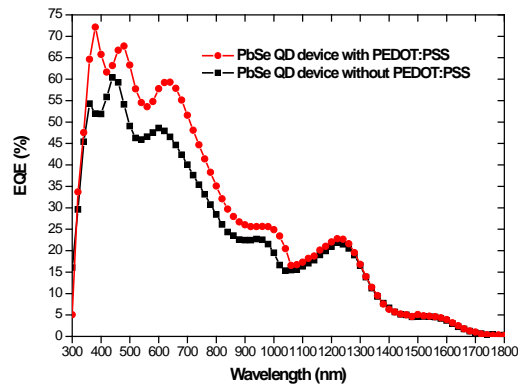


Figure 4. EQE spectra of PbSe QD devices prepared with and without a PEDOT:PSS layer.

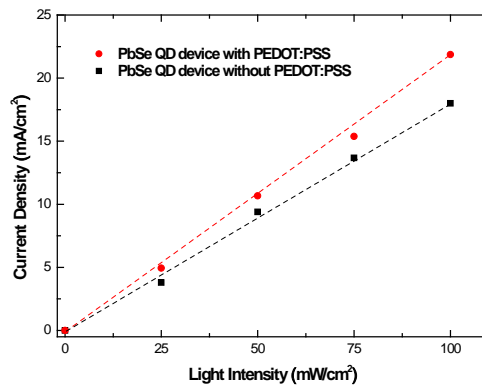


Figure 5. Photocurrent density (J_{sc}) plotted with respect to the intensity of solar light for the PbSe QD device prepared with and without a PEDOT:PSS layer.

Next, we tested the durability of our solar device under simultaneous and continuous AM1.5G illumination and current–voltage scanning. Because PbSe QD–based devices are air-sensitive, with instantaneous degradation having been reported upon their exposure to air,^[19,23] all of our devices were packaged before being measured under ambient conditions. **Figure 6** reveals that the stability of the PCE of the device incorporating the PEDOT:PSS layer was substantially greater relative to that of the device lacking the PEDOT:PSS layer. In particular, the device life times, measured in terms of the time required to reach 80% of the normalized efficiency, for the standard PbSe QD device and the PbSe QD device incorporating the PEDOT:PSS layer were 20 and 120 min, respectively, a six-fold improvement for the latter. Notably, the device incorporating the PEDOT:PSS layer exhibited almost constant values of J_{sc} and FF during its first 60 min of operation; in contrast, its value of V_{oc} decreased

gradually.

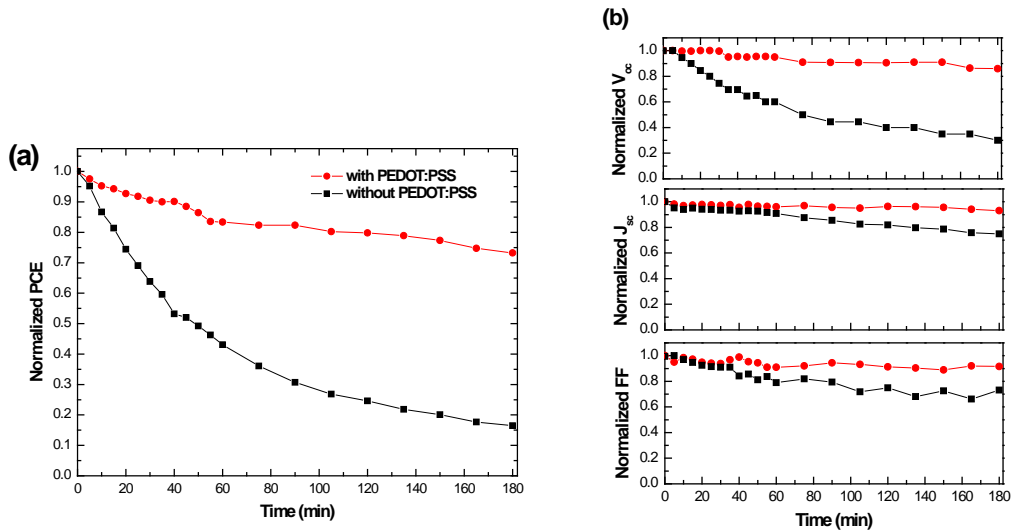


Figure 6. Values of (a) PCE, (b) V_{oc} , J_{sc} , and FF, measured as a function of time and normalized with respect to their initially measured values, for devices prepared with and without a PEDOT:PSS intermediate layer, illuminated continuously under simulated AM1.5G irradiation (100 mW cm^{-2}).

Conclusion

We have prepared photovoltaic devices featuring a PEDOT:PSS hole transport layer and three individually deposited PbSe QD layers. The PbSe photovoltaic devices incorporating the PEDOT:PSS layer exhibited enhanced AM1.5 PCEs relative to those of devices lacking the hole transport layer, with an enhancement factor of 60%. The roughness of the interface between the PEDOT:PSS and PbSe QD layers was almost three times less than that of the original ITO–PbSe QD interface, as measured using X-ray reflectivity. Hence, the presence of the PEDOT:PSS layer not only provided a smoother interface between the PbSe QD layers and the ITO substrate but also resulted in enhanced open-circuit voltages. In addition, the presence of the PEDOT:PSS hole transport layer prolonged the life time, as measured in terms of the time required to reach 80% of the normalized efficiency, of the PbSe QD solar device by six-fold, suggesting that this approach improves the performance of PbSe QD photovoltaic devices.

Experiment:

Materials: Lead(II) oxide (PbO, 99.99%) was obtained from Alfa Aesar. Selenium (Se, 99.9%), oleic acid (OA, tech. 90%), trioctylphosphine (TOP, tech. 90%), 1-octadecene (ODE, tech. 90%), butylamine (BA, 99.5%), and 1,2-ethanedithiol (EDT, 98%) were purchased from Sigma–Aldrich. Octane (HPLC-grade) and acetonitrile (anhydrous) were obtained from TEDIA. Methanol (anhydrous), toluene (anhydrous), and isopropanol (anhydrous) were obtained from J. T. Baker.

PbSe QDs: The QDs were synthesized using standard Schlenk line techniques under an Ar flow; the PbSe used in this study was synthesized according to the method reported by Yu et al^[31]. PbO (0.8920 g, 4.000 mmol), oleic acid (2.825 g, 10.00 mmol), and ODE (12.83 g) were stirred together in a three-neck flask and heated at $160 \text{ }^\circ\text{C}$ under continuous Ar flow for 30 min to obtain a colorless, clear solution. At this temperature, 10% Se-TOP solution (6.4 g) was quickly injected into the solution, dropping the temperature to ca. $150 \text{ }^\circ\text{C}$ for the growth process. After allowing the reaction to proceed for 30–120 s, the mixture was quenched by placing it in a water/ice bath for 1 min. The colloidal QDs were isolated from the growth mixture through repeated precipitations with methanol prior to being dispersed in toluene, vacuum-dried, and stored in a glove box. **Figure 7** displays TEM images of the synthesized PbSe QDs.

BA Ligand Exchange: The ligand exchange process was performed in a N_2 -filled glove box, following the method reported by Konstantatos et al^[32]. The as-synthesized PbSe colloidal QDs were redispersed (to 50 mg mL^{-1}) in anhydrous BA and stirred continuously for 3 days. The resultant QDs were precipitated with anhydrous isopropanol and redispersed in anhydrous octane (80

mg mL⁻¹) for device fabrication. This ligand exchange on the PbSe QDs, albeit completed only partially^[4,33], was designed to improve the quality of their subsequently spin-coated film by reducing the concentration of oleate on the PbSe QDs; after the treatment with butylamine, the domain boundaries in PbSe QDs films are reduced, and a smooth PbSe QDs film was obtained; see **Figure 8**.

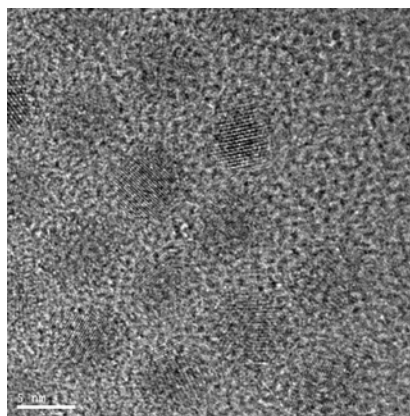


Figure 7. High-resolution transmission electron microscopy image of PbSe QDs capped with oleate ligands. Scale bar: 5 nm. The average size of these PbSe QDs was ca. 5.5 ± 5 nm.

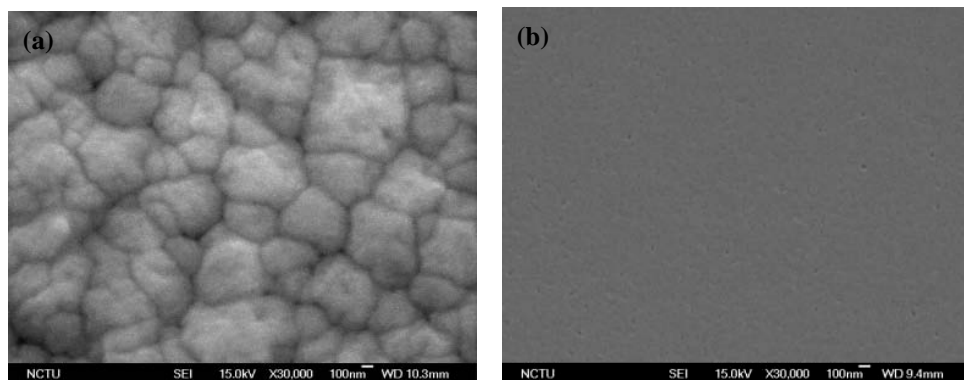


Figure 8. Plan-view scanning electron microscopy image of spin-cast PbSe QD films capped with (a) oleate and (b) butylamine ligands.

Device Fabrication: The patterned ITO on the glass substrate ($5 \Omega \text{ sq.}^{-1}$, Merck) was cleaned through sequential ultrasonic treatment (30 min) with 2% detergent, methanol, acetone, and isopropanol and then dried under a flow of N_2 . PEDOT:PSS (Baytron P VP AI 4083) was then spin-coated on the ultraviolet ozone-treated ITO. After annealing the PEDOT:PSS film at $150 \text{ }^\circ\text{C}$ for 10 min, the PbSe QDs in anhydrous octane were spin-coated onto the PEDOT:PSS layer on the patterned ITO; the samples were then soaked in 0.01 M EDT in anhydrous acetonitrile for several seconds to enhance the film conductivity. The fabrication of the photovoltaic devices involved several steps: (1) the BA-treated PbSe QDs in octane were spin-coated on the PEDOT:PSS layer that had previously been deposited and dried on the ITO electrode; (2) the whole sample, with its surface PbSe QD layer, was treated with 0.01M EDT; (3) the whole sample was rinsed with anhydrous acetonitrile and octane to remove residual free-standing EDT molecules; (4) the treated sample was dried under a stream of N_2 . The resulting PbSe QDs layer is referred herein as PbSe-1. A second layer of EDT-treated PbSe QDs (PbSe-2) was prepared on top of the first by repeating this process. Finally, a third layer of PbSe QDs (PbSe-3) was deposited; together, these three individually spun PbSe QD layers served as the active layer. **Figure 9** presents the Fourier transform IR spectrum of the spin-coated PbSe QD films on the ITO substrates before and after treatment with EDT. The sharp decreases in the intensities of the C–H and COO– signals after EDT treatment indicated that most of the oleate ligands on the PbSe QDs had been removed, because thiol–Pb bonds are much stronger than amine–Pb bonds^[4]. The thickness of the PbSe QD layer was measured using a Dektak profilometer. Finally, 20-nm Ca and 100-nm Al top electrodes were deposited onto all of the samples

at ca. 10^{-7} torr by thermal evaporation through a shadow mask. Four devices were fabricated on each substrate, each with an active area of 0.04 cm^2 .

Characterization: Current density–voltage characteristics of the PbSe QD devices were measured under simulated AM1.5G irradiation (100 mW cm^{-2}) using a Xe lamp–based Newport 66902 150-W solar simulator equipped with a Keithley 236 source measurement unit. The sweeps were performed between +1 and –1 V, with a step size of 0.01 V. For solar cell measurements, the spectrum of the solar simulator was calibrated as follows: A PV-measurement (PVM-154) mono-Si solar cell (NREL calibrated) and a Si photo diode (Hamamatsu S1133) were used to check the irradiation of the exposed area (100 mW cm^{-2}). The mismatch factor ($M = 1.34$) was obtained by using the PVM-154 cell as the reference cell and the fabricated devices as test cells and recording spectra from 300 to 900 nm at intervals of 10 nm. The PVM-154 cell was combined with a KG-5 filter (350–700 nm passed, Newport) to simulate a reference solar cell having spectral responsivity from 350 to 700 nm. The calibration was based on the IEC-69094-1 spectrum. EQE data were recorded with respect to the Optosolar SPF50 spectrum response. A Si reference cell was used to calibrate the wavelengths of light from 300 to 1060 nm, and a Ge reference cell from 1060 to 1800 nm.

Fourier transform infrared (FTIR) spectra were recorded at room temperature using a Perkin–Elmer Spectrum100 instrument. Scanning electron microscopy (SEM) images was acquired using a JEOL JSM-6500F FESEM apparatus operated at accelerating voltages ranging from 5.0 to 15 kV. Transmission electron microscopy (TEM) images were recorded using an FEI Tecnai G2 instrument operated at 200 keV. Synchrotron X-ray reflectivity (XRR) analyses were performed at the wiggler beamline BL-17B1 using an eight-circle diffractometer at the National Synchrotron Radiation Research Center (NSRRC), Hsinchu, Taiwan; the photon energy was 8 keV and the flux was estimated to be $1011 \text{ photons s}^{-1}$. The use of two pairs of slits between the sample and the detector provided a typical wave-vector resolution of ca. 0.001 nm^{-1} in the vertical scattering plane.

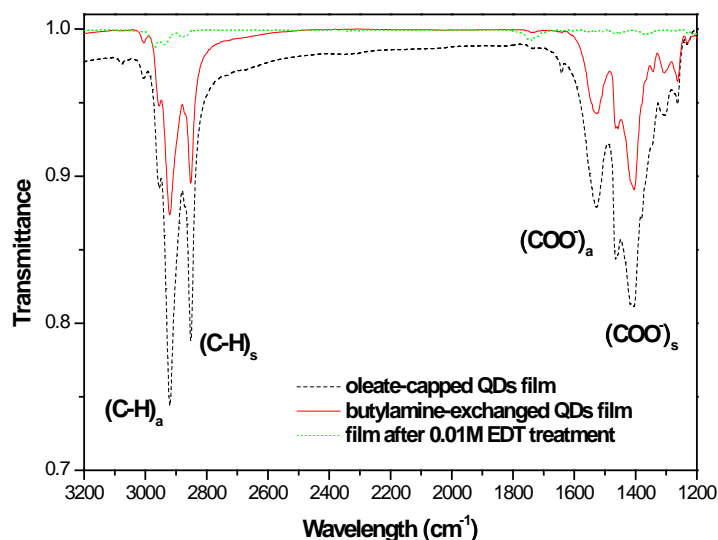


Figure 9. Fourier transform infrared spectra of PbSe QD films: (i) oleate-capped, (ii) butylamine-exchanged, and (iii) butylamine-exchanged with subsequent 0.01 M EDT treatment.

Reference

- [1] J. Y. Kim, K. Lee, N. E. Coates, D. Moses, T. Q. Nguyen, M. Dante, A. J. Heeger, *Science* 2007, 317, 222–225.
- [2] a) L. M. Chen, Z. Hong, G. Li, Y. Yang, *Adv. Mater.* 2009, 21, 1434–1449. b) Y. T. Chang, S. L. Hsu, M. H. Su, K. H. Wei, *Adv. Mater.* 2009, 21, 2093–2097.

- [3] I. Gur, N. A. Fromer, M. L. Geier, A. P. Alivisatos, *Science* 2005, 310, 462–465.
- [4] J. Tang, X. Wang, L. Brzozowski, D. A. R. Barkhosue, R. Debnath, L. Levina, E. H. Sargent, *Adv. Mater.* 2010, 22, 1398–1402.
- [5] D. V. Talapin, C. B. Murray, *Science* 2005, 310, 86–89.
- [6] S. A. McDonald, G. Konstantatos, S. Zhang, P. W. Cyr, E. J. D. Klem, L. Levina, E. H. Sargent, *Nat. Mater.* 2005, 4, 138–142.
- [7] N. Cho, K. R. Choudhury, R. B. Thapa, Y. Sahoo, T. Ohulchanskyy, A. N. Cartwright, K. S. Lee, P. N. Prasad, *Adv. Mater.* 2007, 19, 232–236.
- [8] H. Y. Chen, M. K. F. Lo, G. Yang, H. G. Monbouquette, Y. Yang, *Nature Nanotechnology* 2008, 3, 543–547.
- [9] Z. Tan, T. Zhu, M. Thein, S. Gao, A. Cheng, F. Zhang, C. Zhang, H. Su, J. Wang, R. Henderson, J. Hahn, Y. Yang, J. Xu, *Appl. Phys. Lett.* 2009, 95, 063510.
- [10] a) J. Hou, H. Y. Chen, S. Zhang, R. I. Chen, Y. Yang, Y. Wu, G. Li, *J. Am. Chem. Soc.* 2009, 131, 15586–15587. b) Y. Liang, Z. Xu, J. Xia, S. T. Tsai, Y. Wu, G. Li, C. Ray, L. Yu, *Adv. Mater.* 2010, 22, E135-E138.
- [11] M. A. Hines, G. D. Scholes, *Adv. Mater.* 2003, 15, 1844–1849.
- [12] R. Koole, G. Allan, C. Delerue, A. Meijerink, D. Vanmaekelbergh, A. J. Houtepen, *Small* 2008, 4, 127–133.
- [13] K. Roy Choudhury, Y. Sahoo, T. Y. Ohulchanskyy, P. N. Prasad, *Appl. Phys. Lett.* 2005, 87, 073110.
- [14] M. C. Beard, A. G. Midgett, M. Law, O. E. Semonin, R. J. Ellingson, A. J. Nozik, *Nano Lett.* 2009, 9, 836–845.
- [15] V. Sukhovatkin, S. Hinds, L. Brzozowski, E. H. Sargent, *Science* 2009, 324, 1542–1544.
- [16] R. D. Schaller, V. I. Klimov, *Phys. Rev. Lett.* 2004, 92, 186601.
- [17] J. M. Luther, J. Gao, M. T. Lloyd, O. E. Semonin, M. C. Beard, A. J. Nozik, *Adv. Mater.* 2010, DOI: 10.1002/adma.201001148.
- [18] H. Lee, H. C. Leventis, S. J. Moon, P. Chen, S. Ito, S. A. Haque, T. Torres, F. Nüesch, T. Geiger, S. M. Zakeeruddin, M. Grätzel, Md. K. Nazeeruddin, *Adv. Funct. Mater.* 2009, 19, 2735–2742.
- [19] T. Rauch, M. Böberl, S. F. Tedde, J. Fürst, M. V. Kovalenko, G. Hesser, U. Lemmer, W. Heiss, O. Hayden, *Nature Photonics* 2009, 3, 332–336.
- [20] M. S. Kang, J. Lee, D. J. Norris, C. D. Frisbie, *Nano Lett.* 2009, 9, 3848–3852.
- [21] J. M. Luther, M. Law, Q. Song, C. L. Perkins, M. C. Beard, A. J. Nozik, *ACS Nano* 2008, 2, 271–280.
- [22] G. I. Koleilat, L. Levina, H. Shukla, S. H. Myrskog, S. Hinds, A. G. Pattantyus-Abraham, E. H. Sargent, *ACS Nano* 2008, 2, 833–840.
- [23] J. M. Luther, M. Law, M. C. Beard, Q. Song, M. O. Reese, R. J. Ellingson, A. J. Nozik, *Nano Lett.* 2008, 8, 3488–3492.
- [24] W. Ma, J. M. Luther, H. Zheng, Y. Wu, A. P. Alivisatos, *Nano Lett.* 2009, 9, 1699–1703.
- [25] J. J. Choi, Y. F. Lim, M. B. Santiago-Berrios, M. Oh, B. R. Hyun, L. Sun, A. C. Bartnik, A. Goedhart, G. G. Malliaras, H. D. Abruña, F. W. Wise, T. Hanrath, *Nano Lett.* 2009, 9, 3749–3755.
- [26] K. S. Leschkies, T. J. Beatty, M. S. Kang, D. J. Norris, E. S. Aydil, *ACS Nano* 2008, 3, 3638–3648.
- [27] G. Li, V. Shrotriya, J. Huang, Y. Yao, T. Moriarty, K. Emery, Y. Yang, *Nat. Mater.* 2005, 4, 864–868.
- [28] D. Cui, J. Xu, T. Zhu, G. Paradee, S. Ashok, M. Gerhold, *Appl. Phys. Lett.* 2006, 88, 183111.
- [29] D. M. N. M. Dissanayake, R. A. Hatton, T. Lutz, R. J. Curry, S. R. P. Silva, *Nanotechnology* 2009, 20, 245202.
- [30] L. G. Parratt, *Phys. Rev.* 1954, 95, 359–369.
- [31] W. W. Yu, J. C. Falkner, B. S. Shih, V. L. Colvin, *Chem. Mater.* 2004, 16, 3318–3322.
- [32] G. Konstantatos, I. Howard, A. Fischer, S. Hoogland, J. Cliffod, E. Klem, L. Levina, E. H. Sargent, *Nature* 2006, 442, 180–183.
- [33] M. V. Kovalenko, D. V. Talapin, M. A. Loi, F. Cordella, G. Hesser, M. I. Bodnarchuk, W. Heiss, *Angew. Chem. Int. Ed.* 2008, 47, 3029–3033.

Part II. Ligands Affect the Crystal Structure and Photovoltaic Performance of Thin Films of PbSe Quantum Dots

Abstract: We have prepared thin films of PbSe quantum dots (QDs) featuring three different ligands, oleic acid (OA), butylamine (BA), and 1,2-ethanedithiol (EDT), which have pronounced effects on the arrangement and photovoltaic performance of the PbSe QDs in the thin films. Transmission electron microscopy revealed that ligands that altered the inter-QD spacing induced significant changes in the packing of the PbSe QDs in localized regions of small areas (300×300 nm) of the thin films: from a superlattice of OA-capped PbSe QDs to a chaotic pattern of EDT-capped PbSe QDs. Using a synchrotron X-ray reflectivity probe and data fitting, we determined that the roughnesses decreased and the average densities increased for large-area (1.5×1.5 cm) PbSe QD thin films capped with BA and EDT, relative to those of the OA-capped PbSe QD film. In particular, the PbSe QDs' vertical packing density, which is critical for charge transport, increased substantially for the system incorporating EDT ligands. As a result, devices containing the EDT-treated PbSe QD film as the active layer displayed much improved power conversion efficiencies (PCEs) relative to those of corresponding devices featuring either the OA- or BA-capped PbSe QD films as active layers. Adopting a layer-by-layer technique, we fabricated a EDT-capped PbSe QD device that exhibited a PCE of 2.45%.

Introduction:

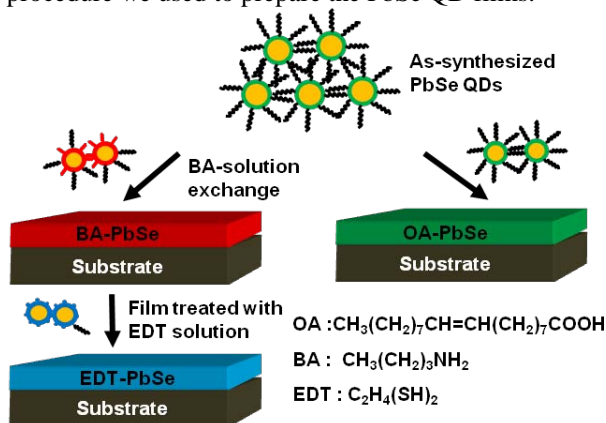
Solution processing of conjugated polymers,¹⁻⁴ organic small molecules,^{5,6} and colloidal quantum dots (QDs)⁷⁻¹³ has many potential benefits, particularly for the rapid and cost-effective preparation of flexible, large-area photovoltaic devices. Solar cells made from polymers typically absorb at wavelengths up to 800 nm, even though the optimal single-junction bandgap of solar cells lies in the region of 1100 nm.¹⁴ An important approach toward realizing significant improvements in performance involves extending the spectral sensitivity of cells to near-infrared wavelengths, which contain as much as half of the energy of the Sun's power spectrum. Such a system can potentially be achieved using Pb-salt colloidal QDs as light-harvesting materials, because their optical bandgap can be tuned to a desired range by virtue of the quantum size.¹⁵⁻¹⁸ Moreover, colloidal Pb-salt QDs can potentially undergo multiple exciton generation,¹⁹⁻²¹ the generation of more than one electron/hole pair, resulting in enhanced photocurrents, which thereby increase the AM1.5 power conversion efficiency (PCE).²²⁻²⁴

The development of Pb-salt colloidal QDs for use in solar cells has undergone rapid advances, becoming a particularly active area of investigation. For example, a PbS QD solar cell featuring a strongly bound bidentate ligand to passivate the PbS QDs, developed through a solution exchange process, has exhibited an AM1.5G PCE of 3.6%.²⁵ Solar cells based on PbSe QD films formed using a layer-by-layer (LBL) technique have exhibited AM1.5G PCEs of 2.1–2.4%.^{26,27} Solar cells based on highly confined ternary $\text{PbS}_x\text{Se}_{1-x}$ QDs have provided a 3.3% AM1.5G PCE.²⁸ Moreover, large improvements in PCEs have been obtained when combining Pb-salt QDs with metal oxide (TiO_2 and ZnO) heterojunctions.²⁹⁻³³

The surfaces of colloidal QDs typically possess long-chain and electrically insulating organic ligands, which must be shortened or removed for use in optoelectronic device applications.^{34,35} A major challenge of current research into colloidal QDs is to devise methods for ligand exchange or chemical treatment with shorter molecules to reduce the inter-QD spacing and, thereby, create more-conductive QD films. Although some studies have been performed in this direction,^{36,37} the influence of ligands on the detailed structure of QD thin films—for example, how the QDs are packed in different directions or the roughness and density of their packing—has never been explored. Structural information relating to QD films is not only of scientific interest; it also provides insight into how the QD films perform as active layers in photovoltaic devices. For example, one of the challenges that must be overcome if we are to employ colloidal QDs in photovoltaic devices is the poor charge transport properties of neat QD films. Rationally achieving this goal requires a deep understanding of the optical, structural, and electronic properties of QD films.

In this study, we investigated the effects of three different ligands—oleic acid (OA), butylamine (BA), and 1,2-ethanedithiol (EDT)—on the structures and photovoltaic performances of PbSe QD films. We used Fourier transform infrared (FTIR) spectroscopy, transmission electron microscopy (TEM), X-ray photoelectron spectroscopy (XPS), and synchrotron grazing incidence X-ray diffraction (GIXRD) to probe the structures of PbSe QDs films capped with these ligands. Additionally, we

measured the current density–voltage characteristics of devices containing these ligand-capped PbSe QD films as active layers to compare their photovoltaic performance. We first synthesized OA-capped PbSe QDs in toluene, precipitating them using centrifugal force. We then added anhydrous BA to perform ligand exchange on the PbSe QDs in solution, again using centrifugal force to obtain BA-PbSe QDs. Suspensions of both the OA- and BA-PbSe QDs in octane were then spin-coated as films onto various substrates for further characterization. Soaking the BA-PbSe QD films on substrates in EDT solution for a short period of time provided EDT-PbSe QD films. **Scheme 1** depicts the procedure we used to prepare the PbSe QD films.



Scheme 1 Fabrication of PbSe QD thin films incorporating various ligands.

Experiment:

Materials.

Lead(II) oxide (PbO, 99.9%), selenium (Se, 99.9%), OA (tech. 90%), trioctylphosphine (TOP, tech. 90%), 1-octadecene (ODE, tech. 90%), and BA (99.5%) were purchased from Sigma–Aldrich. EDT (>98%) was acquired from Fluka. Anhydrous octane, MeCN, MeOH, toluene, isopropanol, and tetrachloroethylene (TCE, 99.9%) were obtained from J. T. Baker.

PbSe QDs.³⁸

PbO (0.8920 g, 4.00 mmol) was dissolved in a mixture of OA (2.825 g, 10.00 mmol) and ODE (12.83 g) in a three-necked flask and heated at 165 °C under vigorous stirring and a continuous Ar flow for 45 min to obtain a colorless, clear solution. At this temperature, 10% Se-TOP solution (6.4 g) was rapidly injected into the solution, dropping the temperature to ca. 150 °C for the growth process. Typically, 4.5-nm colloidal QDs were obtained after allowing the reaction to proceed for 45 s; cold toluene was injected into the mixture to terminate the reaction. The colloidal QDs were subsequently isolated from the growth mixture through repeated precipitations with MeOH prior to dispersal in toluene to remove any excess of unreacted ligands.

BA Solution Ligand Exchange.³⁹

The as-synthesized PbSe colloidal QDs were redispersed in anhydrous BA solution and stirred continuously for 48 h in a N₂-filled glove box. The BA-exchanged QDs were precipitated with anhydrous isopropanol, dried, and redispersed in anhydrous octane.

QD Films.

All processing was performed in a N₂-filled glove box. PbSe colloidal QDs were spin-coated from octane (80 mg mL⁻¹) onto various substrates, including polished Si substrates, indium tin oxide (ITO), and copper grids fixed on glass substrates. The BA-exchanged QDs films were then soaked in a 1 mM EDT in MeCN for several seconds before being rinsed with anhydrous MeCN to remove any residual free-standing EDT.

Material Characterization.

Attenuated total reflection Fourier transform infrared (ATR-FTIR) spectra were recorded at room temperature using a Perkin–Elmer Spectrum100 spectrometer. Optical absorption data were

acquired using a Hitachi U-4100 spectrophotometer equipped with an integrating sphere. XPS was performed using a Thermo VG Scientific Microlab 350 instrument, monochromated Mg K α radiation, and a pass energy of 29 eV. TEM images were recorded using an FEI Spirit TWIN instrument operated at 120 keV. The surface normal wide-angle X-ray scattering (WAXS) and in-plane GIXRD measurements at high resolution were performed at the wiggler beamline BL-17B1 using an eight-circle diffractometer in the National Synchrotron Radiation Research Center (NSRRC), Hsinchu, Taiwan. For GIXRD and WAXS analyses, the photon energy was 8 keV with a flux estimated to be 10^{11} photons s $^{-1}$. Use of two pairs of slits between the sample and the detector provided a typical wave-vector resolution of ca. 0.001 nm $^{-1}$ in the vertical scattering plane in this experiment.

Device Fabrication and Characterization.

The patterned ITO on the glass substrate (5 Ω sq. $^{-1}$, Merck) was cleaned through sequential ultrasonic treatment with detergent, MeOH, acetone, and isopropanol and then dried under a flow of N $_2$. Poly(3,4-ethylenedioxythiophene):poly(styrene sulfonate) (PEDOT:PSS; Baytron P VP AI 4083) was then spin-coated on the UV ozone-treated ITO; the sample was annealed at 150 $^{\circ}$ C for 1 h before being transferred to a N $_2$ -filled glove box. For the OA-capped and BA-exchanged PbSe QD devices, the QDs in octane were spin-coated on the PEDOT:PSS layer that had previously been deposited on the ITO electrode. For the EDT-treated QD device, the BA-exchanged QD film on the ITO electrode was soaked in 1 mM EDT for 5 s. Moreover, using the LBL technique, the BA-exchanged QD solution (50 mg mL $^{-1}$) was spin-coated on the PEDOT:PSS/ITO substrate and then the whole sample was treated with 1 mM EDT, rinsed with anhydrous MeCN and octane, and dried under a stream of N $_2$; these steps were repeated for four cycles. All the active layers were typically 120 ± 20 nm thick, as measured using a Veeco Dektak profilometer. Finally, 20-nm Ca and 100-nm Al top electrodes were deposited onto all of the samples at ca. 10^{-7} torr by thermal evaporation through a shadow mask. Four devices were fabricated on each substrate, each with an active area of 0.04 cm 2 .

Current density–voltage characteristics of the PbSe QD devices were measured by illuminating these devices through a mask that fits⁴⁰ the electrode crossing area under simulated AM1.5G irradiation (100 mW cm $^{-2}$) using a Xe lamp-based Newport 66902 150-W solar simulator equipped with a Keithley 2400 source measurement unit. For solar cell measurements, the spectrum of the solar simulator was calibrated as follows:⁴¹ A PV-measurement (PVM-154) mono-Si solar cell (NREL calibrated) and a Si photo diode (Hamamatsu S1133) were used to check the irradiation of the exposed area (100 mW cm $^{-2}$). A mismatch factor ($M = 1.34$) was obtained when using the PVM-154 cell as the reference cell and the fabricated devices as test cells and recording spectra from 300 to 900 nm at intervals of 10 nm. The PVM-154 cell was combined with a KG-5 filter (350–700 nm passed, Newport) to simulate a reference solar cell having spectral responsivity from 350 to 700 nm. The calibration was based on the IEC-69094-1 spectrum. External quantum efficiency (EQE) data were recorded with respect to the Optosolar SPF50 spectrum response. A Si reference cell was used to calibrate the wavelengths of light from 300 to 1060 nm; a Ge reference cell, from 1060 to 1800 nm.

Results and Discussion: **Figure 1a** presents FTIR spectra of PbSe QD films that had experienced treatment with the different ligands; these spectra confirm the nature of the chemical species on the surfaces of the PbSe QD films. We subjected the films of the OA-capped PbSe QDs to two different ligand treatment processes: (i) BA-exchange and (ii) BA-exchange with subsequent EDT treatment. The presence of signals for COO $^{-}$ stretching at 1400 and 1530 cm $^{-1}$ in the FTIR spectrum of the BA-capped QD film indicates that some of the OA units had been removed; a comparison of the area under the COO $^{-}$ stretching region in the FTIR spectrum of the OA-capped PbSe QDs to that of the BA-exchanged PbSe QD film reveals that 14% of the OA ligands had been removed during the mixing process in anhydrous BA. The spectrum of the BA-exchanged QD film features a weak signal in the range 3250–3400 cm $^{-1}$, indicating the presence of amino groups. This BA ligand exchange on the PbSe QDs, albeit completed only partially, was designed to improve the quality of subsequently spin-coated PbSe QD films by reducing the domain boundaries in the PbSe QDs films, resulting in a smoother BA-exchanged PbSe QD film relative to that of the initially prepared oleate-capped PbSe QDs. Moreover, the intensities of the signals for both the COO $^{-}$ and C–H units were dramatically reduced in the spectrum of the EDT-treated PbSe QD film, indicating that most of the OA ligands on the PbSe QDs had been exchanged, because thiol–Pb bonds are much stronger than amine–Pb or carboxyl–Pb bonds.⁴² Further evidence to support this argument was provided by the appearance of a signal for the S–C bonds of the EDT ligands at 650–680 cm $^{-1}$ in the spectrum.

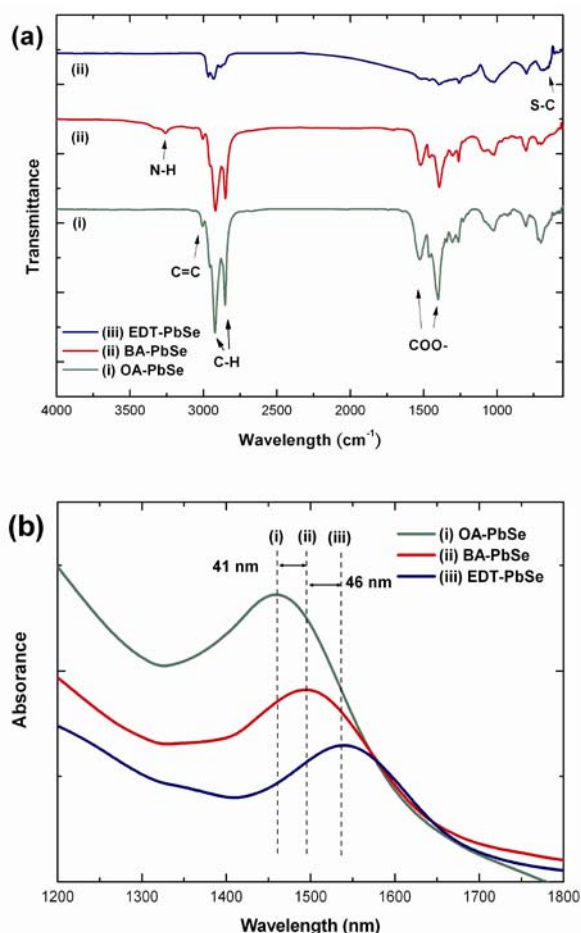


Fig. 1 (a) ATR-FTIR spectra and (b) optical absorption spectra of PbSe QD films capped with (i) OA, (ii) BA, and (iii) EDT, prepared through spin-coating onto substrates. Average size of PbSe QDs: 4.6 nm.

Figure 1b displays absorption spectra of the PbSe QD films capped with the various ligands. The first exciton absorption peak of OA-capped QD film was located at 1455 nm; the average size of the PbS QDs was 4.6 nm, as estimated from the TEM image. Because the absorption spectra of the PbSe QD films were similar to that of the PbSe QDs in tetrachloroethylene (data not shown), we can calculate the sizes of the PbSe QDs using Equation (1), which describes the dependence of a PbSe QDs' particle size on the position of its first absorption peak in solution:⁴³

$$D = (\lambda - 143.75) / 281.25 \quad (1)$$

where D (nm) is the average particle diameter of the PbSe QDs and λ (nm) is the first absorption peak position of the corresponding sample. The estimated size (4.6 nm) for the PbSe QDs is in good agreement with the diameter calculated (4.66 nm) for the PbSe QDs using equation (1). Moreover, the BA-treated PbSe QD film and the PbSe QD film subsequently treated with EDT exhibited their first exciton absorption peaks at 1496 and 1542 nm, respectively. Thus, red-shifts of 41 and 87 nm, respectively, relative to the signal for the OA-capped QD film, imply higher packing densities for the BA- and EDT-ligated PbSe QD films, presumably because of strengthened dipole-dipole interactions and cross-linking of the QDs, respectively. Such interactions reduce the inter-QD distances, in turn leading to increased PbSe QD packing densities and conductivities.⁴⁴

We used XPS to detect the presence of elemental species on the surfaces of the PbSe QD films. **Figure 2a** reveals a strong signal for oxygen atoms and a weak signal for carbon atoms at binding energies of 531 and 287.8 eV, respectively, in the spectrum of the OA-capped QD films; we assign

them to the oxygen and carbon atoms of the carboxylate groups of OA units. Moreover, we assign a signal for carbon atoms at 284.7 eV to the alkyl chains of the OA units. The slight decreases in intensity of the signals for the oxygen and carbon atoms on the BA-exchanged QD film are consistent with the partial removal of OA ligand from the PbSe QD surface. The nitrogen atom spectrum of the BA-exchanged QD film features a signal at 399.1 eV, revealing the presence of the amino groups of the BA units. The simultaneous lack of signals for oxygen atoms and the decreased intensities of the signals for carbon atoms on the EDT-treated films are consistent with the fact that the OA ligands were removed. Moreover, the EDT-treated films revealed a signal for sulfur atoms at 161.8 eV, consistent with sulfur atoms bound to the PbSe QD surfaces as thiolate species.

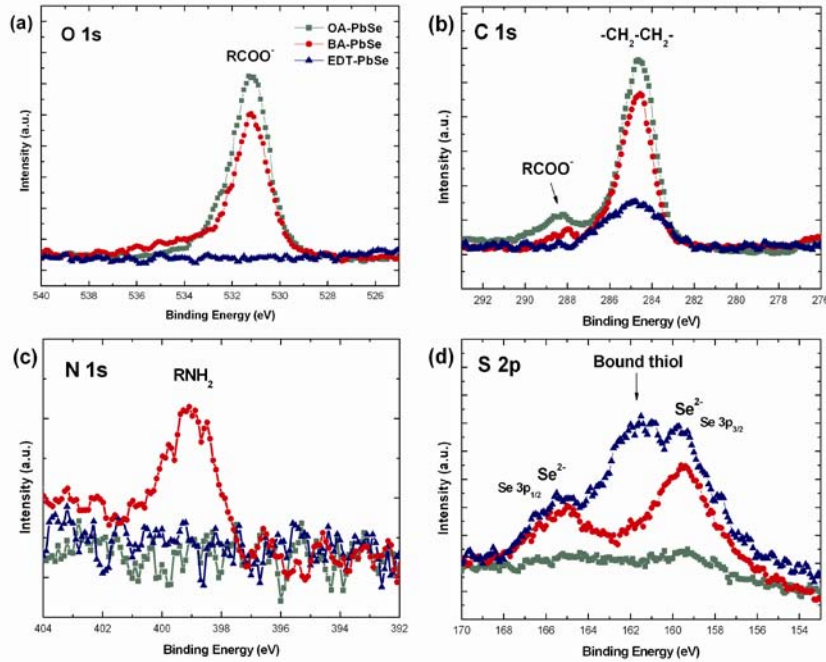


Fig. 2 XPS spectra of PbSe QD films capped with OA (green squares), BA (red circles), and EDT (blue triangles). The samples were spin-cast onto Si substrates and measured without exposure to air.

Figure 3 displays TEM images, with (100) projections, of localized regions of the OA-capped, BA-exchanged, and EDT-treated PbSe QDs films. **Figure 3a** presents the TEM image of the OA-capped film, revealing a large area of ordered PbSe QDs in a square assembly, exhibiting three-dimensional (3D) superlattices that had nucleated simultaneously and grown together on the Cu grids. The fast Fourier transform (FFT) image of the OA-PbSe QDs (inset to **Figure 3a**) reveals a four-fold symmetry within the 3D ordered superlattice, consistent with the square assembly pattern of PbSe QDs in the TEM image. It has been reported that PbSe QDs form hexagonal assemblies when processed at a concentration of ca. 0.5–5.0 mg mL⁻¹.⁴⁵ We suspect that our large-area square assembly of QDs formed because we performed the spin-coating processing at a higher PbSe QD concentration. When we changed the concentration of the OA-treated PbSe QD solution or the film environment, the morphology of the film could become quite different; the TEM image in **Figure 4a**, of a film obtained using a diluted PbSe QD solution (50 mg mL⁻¹), reveals a square assembly of PbSe QDs within the thicker region of the film, whereas the surrounding thinner region features a hexagonal assembly. **Figure 3b** presents TEM images of the film of the OA-capped PbSe QD superlattice after exposure to air; the QD superlattices transformed into a mostly hexagonal assemblies after exposure for 2 days. **Figure 3c** displays a TEM micrograph of the BA-capped PbSe QDs, revealing some ordered and disordered domains, due to the partial removal of OA after BA solution exchange. **Figure 3c** presents a TEM image of the EDT-treated PbSe QDs; this film featured a chaotic phase because of a loss of free volume during the EDT treatment process, leading to stress buildup and the formation of disordered domains, having an average size of ca. 100 nm, in the regions. The FFT image in the inset to **Figure 3c** reveals vague square symmetry, indicating that the superlattice domain of the PbSe QDs film was destroyed and had become chaotic.

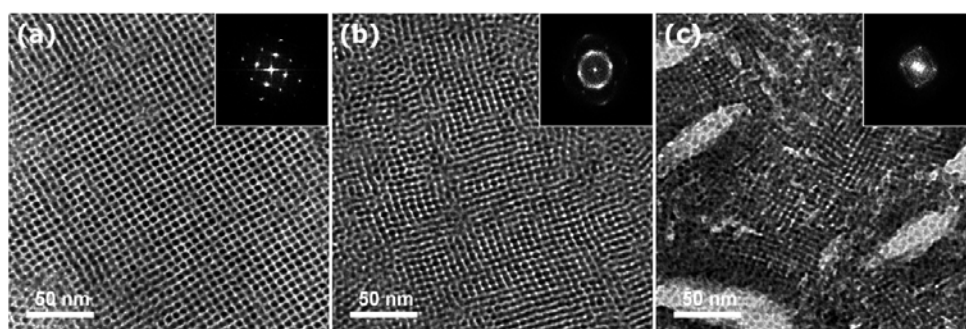


Fig. 3 TEM images of the 3D arranged superlattices of PbSe QDs films capped with (a) OA, (b) BA, and (c) EDT with (100) projections of lattices (scale: 50 nm). Insets: Corresponding FFT patterns revealing the ordering of the superlattices. The samples were prepared by spin-coating PbSe QD solutions (concentration: 80 mg mL^{-1}) onto Cu grids fixed on glass substrates under an inert atmosphere.

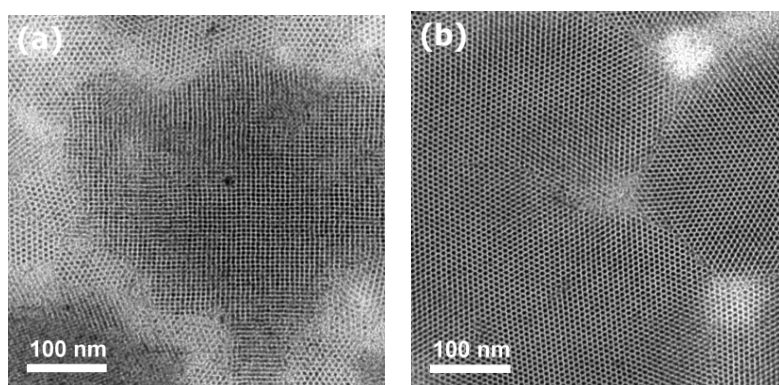


Figure 4. TEM images of the superlattices of the OA-capped PbSe QD film (a) before and (b) after exposure to air for 2 days; scale: 100 nm. The sample was prepared through spin-coating of a solution of PbSe QD (50 mg mL^{-1}) in octane in a N_2 -filled glove box.

Figure 5a presents synchrotron X-ray radial scans recorded along the surfaces normal to the spin-coated PbSe QD films capped with OA, BA, and EDT on Si substrates. The solid line is the fitted curve of the XRR part in the radial-scan data. Our simulation of the specular reflectivity, allowing us to acquire the physical parameters of the multilayer, was based on the recursive formalism of Parratt;⁴⁶ we then fitted the reflectivity data with the Bede_{REFS} Mercury code⁴⁷ to determine the physical parameters of the multilayer, including its roughness, thickness, and density. In **Figure 5a**, the XRR fitting curves of the BA- and EDT-treated PbSe QD films exhibit more striking oscillations than that of the OA-capped PbSe QD film, providing direct evidence that treatment of the PbSe QDs with BA and EDT decreased the roughness of the films. From the fitted data, we obtained a roughness of 8.0 nm for the PbSe QD film capped with OA; this value was only 3.8 nm for both the BA-exchanged and EDT-treated PbSe QD films—almost a two-fold improvement with respect to that of the original QD film. Furthermore, the critical angle of total reflection, as indicated by the dashed line, increased substantially—implying increases in the average film density—after we treated the PbSe QDs with BA or EDT. The fitted densities for the OA-capped, BA-capped, and EDT-treated PbSe QD films were 1.86, 3.56, and 4.69 g cm^{-3} , respectively. Treatment of the BA-exchanged PbSe QD film with EDT caused the thickness of the resulting film to decrease from 62 to 45 nm, with an associated increase in the film density. In **Figure 5a**, the first peaks, as indicated by the arrows and corresponding to the first-order Bragg diffraction from the films, shifted toward higher values of q when the PbSe QDs were treated with BA or EDT, revealing smaller inter-particle spacings in the packing directions along the surface normal of the films. Specifically, BA-exchange reduced the surface-normal d -spacing (d_z) from 6.83 to 5.92 nm, consistent with partial removal of the OA ligands. Treatment with EDT further removed most of the OA ligands and resulted in a surface-normal value

of d_z of 4.72 nm, the largest decrease in all cases. The broadness of the first peaks of the BA-exchanged and EDT-treated films indicated that such chemical treatment destroyed the superlattice ordering of the OA-treated PbSe QD films as a result of the layers of PbSe QDs distorting during OA removal. **Figure 5b** displays the X-ray in-plane crystal-truncation-rod (CTR) along the (H 0 0) direction. For the PbSe QD films capped with OA and BA, the d -spacings in the x direction were quite similar; the value of q_z was 0.87 nm^{-1} ($d_x = 7.22 \text{ nm}$) for the former and 0.85 nm^{-1} ($d_x = 7.39 \text{ nm}$) for the latter. For the PbSe QD film capped with EDT, however, the values of the surface-normal d_z and in-plane d_x decreased to 4.72 and 6.48 nm, respectively, from 6.83 and 7.22 nm, respectively, for the OA-capped PbSe QD film.

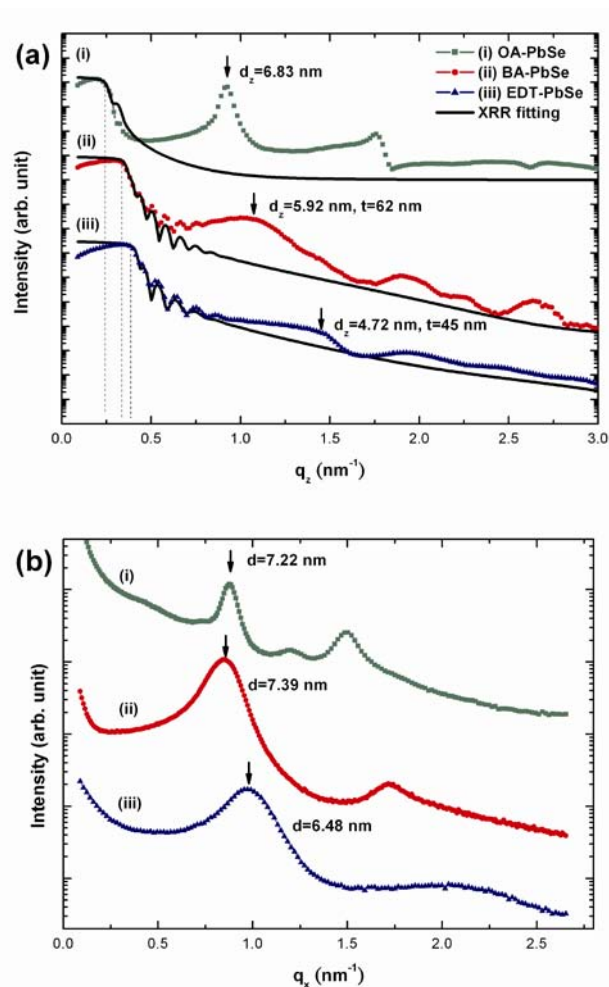


Fig. 5 Profiles of (a) the synchrotron X-ray radial scans along the surface normal and XRR fitting and (b) the in-plane CTR scans of (i) OA-, (ii) BA-, and (iii) EDT-capped PbSe QD films, prepared through spin-coating onto Si substrates (log-normal scale).

Furthermore, the azimuthal scan (Phi scan) of these QDs films (**Figure 6**) all display fourfold symmetry, implying that the PbSe QD films maintained square assembled structures in the ab plane, consistent with the TEM results. Moreover, there was little difference between the in-plane CTR and azimuthal scans of the PbSe QD films when using either ITO/PEDOT:PSS or Si substrates (**Figure 7**); that is, there was no substrate effect on the structure of the PbSe QDs films. **Table 1** lists the synchrotron X-ray characteristics of the PbSe QD films capped with OA, BA, and EDT.

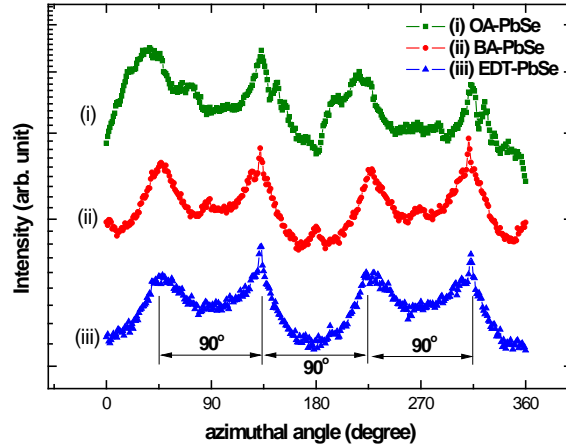


Figure 6. Synchrotron X-ray azimuthal scans of (i) OA-, (ii) BA-, and (iii) EDT-capped PbSe QD films, prepared through spin-coating onto Si substrates (log-normal scale).

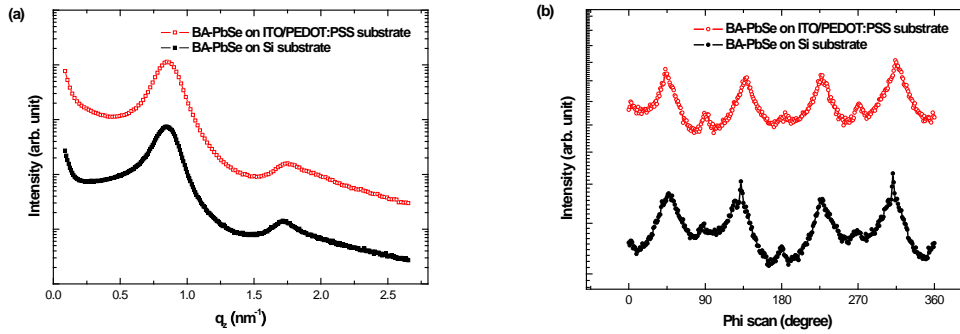


Figure 7. Synchrotron X-ray (a) in-plane CTR and (b) azimuthal scans of BA-capped PbSe QD films, prepared by spin-coating onto ITO/PEDOT:PSS and Si substrates.

Table 1. Data from synchrotron X-ray radial scans along the surface normal and in-plane crystal-truncation-rod scans of the ligand-capped PbSe QD films. Average size of PbSe QDs: 4.6 nm.

	OA-PbSe	BA-PbSe	EDT-PbSe
Thickness (nm)	140	62	45
Roughness (nm)	8	3.8	3.8
Average density of film (g cm^{-3})	1.86	3.56	4.69
Surface-normal d -space (nm)	6.83	5.92	4.72
In-plane d -space (nm)	7.22	7.39	6.48
Ordering of superlattice	good	poor	very poor

Figure 8 presents current density–voltage plots of the ligand-treated PbSe QD devices, each incorporating a thin PEDOT:PSS hole transport layer to improve the photovoltaic performance and stability.²⁷ The thickness of the active layer in each of these QD devices was 120 ± 20 nm, as measured using a profile-meter. The spin-casted OA-capped QD device exhibited very poor photovoltaic performance because of the low electrical conductivity of the 18-carbon-atom chains of the OA ligands (ca. 2 nm) on the PbSe QDs. For the BA-exchanged QD device, the short-circuit current density (J_{sc}), open-circuit voltage (V_{oc}), and fill factor (FF) were 1.58 mA cm^{-2} , 0.23 V, and 0.39, respectively. For the EDT-treated QD device, the values of J_{sc} and V_{oc} and the FF were 15.0

mA cm^{-2} , 0.16 V, and 0.37, respectively. As expected, the values of J_{sc} of the BA-exchanged and EDT-treated QD devices were significantly higher than that of the OA-capped PbSe QD device; indeed, the value of J_{sc} of the EDT-treated QD device was approximately nine times greater than that of the BA-exchanged QD device. The increase in the value of J_{sc} of the device incorporating the EDT-treated PbSe QD film resulted from this thiol-terminated cross-linker decreasing the interparticle spacing and increasing the film density; the decrease in V_{oc} was due to a decrease in the thickness of the QD film.

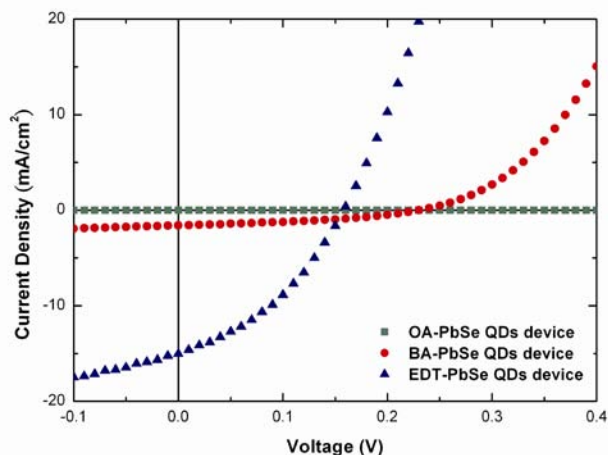


Fig. 8 Current–voltage characteristics of the ligand-capped PbSe QD devices on ITO/PEDOT:PSS substrates: OA-capped, BA-exchanged, and BA-exchanged with subsequent 1 mM EDT treatment for 5 s. The devices were illuminated under AM1.5G conditions (100 mW cm^{-2}).

Table 2. Photovoltaic parameters of PbSe QD devices measured under solar illumination. Device structure: ITO/PEDOT:PSS/PbSe QDs/Ca/Al.

	V_{oc}^a (V)	J_{sc}^b (mA cm^{-2})	FF ^c (%)	η^d (%)
OA-capped film	–	–	–	–
BA-exchanged film	0.23	1.58	39	0.14
EDT-treated film	0.16	15.0	37	0.89
EDT-treated film (LBL)	0.22	26.4	42	2.45

^a V_{oc} : Open-circuit voltage. ^b J_{sc} : Short-circuit current density. ^c FF: Fill factor. ^d η : PCE. Solar: AM1.5G (100 mW cm^{-2}).

To further improve the photovoltaic performance of the PbSe QD devices, we optimized the device fabrication procedure using a LBL technique, with an intermediate BA ligand-exchange step in solution prior to EDT treatment of the films in the solid state. **Figure 9a** displays the current density–voltage characteristics of a device incorporating a $110 \pm 10 \text{ nm}$ –thick layer of 4.6-nm-diameter PbSe QDs measured at room temperature in N_2 -filled glove box under AM 1.5G conditions. The device exhibiting the highest performance—a maximum AM 1.5G PCE of 2.45%—was prepared using four deposition cycles of PbSe QDs on an ITO/PEDOT:PSS substrate. **Table 2** lists the photovoltaic performance parameters of these PbSe QD devices under solar illumination. **Figure 9b** presents the EQE curve for best-performing PbSe QD device over the wavelength region from 300 to 1800 nm, covering the entire visible light range and a small portion of the near-infrared. The theoretical short-circuit current density, obtained after integrating the EQE curve, for this device was 23.6 mA cm^{-2} ; this value is close to that (26.4 mA cm^{-2}) obtained directly from the I – V curves, confirming the accuracy of our measurements.

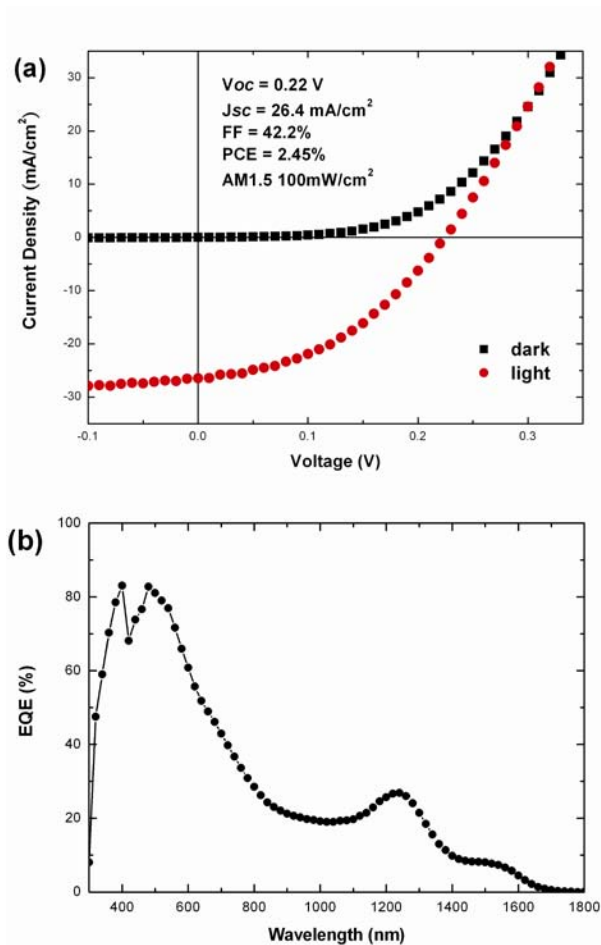


Fig. 9 (a) Current–voltage characteristics and (b) EQE spectrum of the EDT-capped PbSe QD device prepared on an ITO/PEDOT:PSS substrate using the LBL technique, under AM1.5G irradiation (100 mW cm^{-2}).

Conclusions

The ligands OA, BA, and EDT affect the assembly and photovoltaic performance of PbSe QDs deposited in the form of thin films. Changes in the interparticle spacing induced by these ligands significantly influenced the ordering of the PbSe QD films, from superlattices to chaotic patterns. For PbSe QD films capped with BA and EDT, the roughness decreased and the average density increased relative to those of the OA-capped PbSe QD film. In particular, the vertical packing of the PbSe QDs, critical for charge transport, increased substantially after treatment with EDT. As a result, the PCE of a device containing the EDT-treated PbSe QD film as the active layer was much greater than that of the corresponding OA-capped PbSe QD device. Moreover, applying an LBL fabrication technique enhanced the PCE of a PbSe QD device to 2.45%.

Reference

- [1] J. Y. Kim, K. Lee, N. E. Coates, D. Moses, T. Q. Nguyen, M. Dante, and A. J. Heeger, *Science*, 2007, 317, 222–225.
- [2] H. Y. Chen, J. Hou, S. Zhang, Y. Liang, G. Yang, Y. Yang, L. Yu, Y. Wu, and G. Li, *Nature Photonics*, 2009, 3, 649–653.
- [3] W. J. E. Beek, M. M. Wienk, and R. A. J. Janssen, *J. Mater. Chem.*, 2005, 15, 2985–2988.

- [4] J. C. Hindson, B. Ulgut, R. H. Friend, N. C. Greenham, B. Norder, A. Kotlewski, and T. J. Dingemans, *J. Mater. Chem.*, 2010, 20, 937-944.
- [5] P. Peumans, S. Uchida, and S. R. Forrest, *Nature*, 2003, 425, 158-162.
- [6] F. Odobel, E. Blart, M. Lagr e, M. Villieras, H. Boujtita, N. El Murr, S. Caramori, and C. Alberto Bignozzi, *J. Mater. Chem.*, 2003, 13, 502-510.
- [7] S. A. McDonald, G. Konstantatos, S. Zhang, P. W. Cyr, E. J. D. Klem, L. Levina, and E. H. Sargent, *Nat. Mater.*, 2005, 4, 138-142.
- [8] W. A. Tisdale, K. J. Williams, B. A. Timp, D. J. Norris, E. S. Aydil, and X. Y. Zhu, *Science*, 2010, 328, 1543-1547.
- [9] I. Gur, N. A. Fromer, M. L. Geier, and A. P. Alivisatos, *Science*, 2005, 310, 462-465.
- [10] M. T. Zin, A. M. Munro, M. Gungormus, N. Y. Wong, H. Ma, C. Tamerler, D. S. Ginger, M. Sarikaya, and A. K.-Y. Jen, *J. Mater. Chem.*, 2007, 17, 866-872.
- [11] M. Law, J. M. Luther, Q. Song, B. K. Hughes, C. L. Perkins, and A. J. Nozik, *J. Am. Chem. Soc.*, 2008, 130, 5974-5985.
- [12] A. Kongkanand, K. Tvrdy, K. Takechi, M. Kuno, and P.V. Kamat, *J. Am. Chem. Soc.*, 2008, 130, 4007-4015.
- [13] B. Sun, and N. C. Greenham, *Phys. Chem. Chem. Phys.*, 2006, 8, 3557-3560.
- [14] C. H. Henry, *J. Appl. Phys.*, 1980, 51, 4494-4500.
- [15] K. R. Choudhury, Y. Sahoo, T. Y. Ohulchanskyy, and P. N. Prasad, *Appl. Phys. Lett.*, 2005, 87, 073110.
- [16] K. Szendrei, W. Gomulya, M. Yarema, W. Heiss, and M. A. Loi, *Appl. Phys. Lett.*, 2010, 97, 203501.
- [17] K. R. Choudhury, D. W. Song, and F. So., *Organic Electronics*, 2010, 11, 23-28.
- [18] M. A. Hines, and G. D. Scholes, *Adv. Mater.*, 2003, 15, 1844-1849.
- [19] V. Sukhovatkin, S. Hinds, L. Brzozowski, and E. H. Sargent, *Science*, 2009, 324, 1542-1544.
- [20] M. C. Beard, A. G. Midgett, M. Law, O. E. Semonin, R. J. Ellingson, and A. J. Nozik, *Nano Lett.*, 2009, 9, 836-845.
- [21] M. Ji, S. Park, S. T. Connor, T. Mokari, Y. Cui, and K. J. Gaffney, *Nano Lett.*, 2009, 9, 1217-1222.
- [22] R. D. Schaller, and V. I. Klimov, *Phys. Rev. Lett.*, 2004, 92, 186601.
- [23] J. Tang, X. Wang, L. Brzozowski, D. A. R. Barkhouse, R. Debnath, L. Levina, and E. H. Sargent, *Adv. Mater.*, 2010, 22, 1-5.
- [24] N. Cho, K. R. Choudhury, R. B. Thapa, Y. Sahoo, T. Ohulchanskyy, A. N. Cartwright, K.S. Lee, and P. N. Prasad, *Adv. Mater.*, 2007, 19, 232-236.
- [25] R. Debnath, J. Tang, D. A. Barkhouse, X. Wang, A. G. Pattantyus-Abraham, L. Brzozowski, L. Levina, and E. H. Sargent, *J. Am. Chem. Soc.*, 2010, 132, 5952-5953.
- [26] J. M. Luther, M. Law, M. C. Beard, Q. Song, M. O. Reese, R. J. Ellingson, and A. J. Nozik, *Nano Lett.*, 2008, 8, 3488-3492.
- [27] C. Y. Kuo, M. S. Su, Y. C. Hsu, H. N. Lin, and K. H. Wei, *Adv. Funct. Mater.*, 2010, 20, 3555-3560.
- [28] W. Ma, J. M. Luther, H. Zheng, Y. Wu, and A. P. Alivisatos, *Nano Lett.*, 2009, 9, 1699-1703.
- [29] J. M. Luther, J. Gao, M. T. Lloyd, O. E. Semonin, M. C. Beard, and A. J. Nozik, *Adv. Mater.*, 2010, 22, 3704-3707.
- [30] A. G. Pattantyus-Abraham, I. J. Kramer, A. R. Barkhouse, X. Wang, G. Konstantatos, R. Debnath, L. Levina, I. Raabe, M. K. Nazeeruddin, M. Gr tzel, and E. H. Sargent, *ACS Nano*, 2010, 4, 3374-3380.
- [31] J. J. Choi, Y. F. Lim, M. B. Santiago-Berrios, M. Oh, B. R. Hyun, L. Sun, A. C. Bartnik, A. Goedhart, G. G. Malliaras, H. D. Abru a, F. W. Wise, and T. Hanrath, *Nano Lett.*, 2009, 9, 3749-3755.
- [32] K. S. Leschkies, T. J. Beatty, M. S. Kang, D. J. Norris, and E. S. Aydil, *ACS Nano*, 2008, 3, 3638-3648.
- [33] T. Ju, R. L. Graham, G. Zhai, Y. W. Rodriguez, A. J. Breeze, L. Yang, G. B. Alers, and S. A. Carter, *Appl. Phys. Lett.*, 2010, 97, 043106.
- [34] D. V. Talapin, and C. B. Murray, *Science*, 2005, 310, 86-89.
- [35] Y. Liu, M. Gibbs, J. Puthussery, S. Gaik, R. Ihly, H. W. Hillhouse, and M. Law, *Nano Lett.*, 2010, 10, 1960-1969.
- [36] M. V. Kovalenko, M. Scheele, and D. V. Talapin, *Science*, 2009, 324, 1417-1420.
- [37] K. Szendrei, D. Jarzab, M. Yarema, M. Sytnyk, S. Pichler, J. C. Hummelen, W. Heiss, and M. A. Loi, *J. Mater. Chem.*, 2010, 20, 8470-8473.

- [38] W. W. Yu, J. C. Falkner, B. S. Shih, and V. L. Colvin, *Chem. Mater.*, 2004, 16, 3318–3322.
- [39] G. Konstantatos, I. Howard, A. Fischer, S. Hoogland, J. Clifford, E. Klem, L. Levina, and E. H. Sargent, *Nature*, 2006, 442, 180–183.
- [40] A. Cravino, P. Schilinsky, and C. J. Brabec, *Adv. Funct. Mater.*, 2007, 17, 3906–3910.
- [41] M. Y. Chiu, U. S. Jeng, C. H. Su, K. S. Liang, and K. H. Wei, *Adv. Mater.*, 2008, 20, 2573–2578.
- [42] M. V. Kovalenko, D. V. Talapin, M. A. Loi, F. Cordella, G. Hesser, M. I. Bodnarchuk, and W. Heiss, *Angew. Chem. Int. Ed.*, 2008, 47, 3029–3033.
- [43] Q. Dai, Y. Wang, X. Li, Y. Zhang, D. J. Pellegrino, M. Zhao, B. Zou, J. Seo, Y. Wang, and W. W. Yu, *ACS Nano*, 2009, 3, 1518–1524.
- [44] G. Sarasqueta, K. R. Choudhury, and F. So, *Chem. Mater.*, 2010, 22, 3496–3501.
- [45] T. Hanrath, J. J. Choi, and D. M. Smilgies, *ACS Nano*, 2009, 3, 2975–2988.
- [46] L. G. Parratt, *Phys. Rev.*, 1954, 95, 359–369.
- [47] D. K. Bowen, and B. K. Tanner, *Nanotechnology*, 1993, 4, 175–182.

Part III.

Annealing Treatment Improves the Morphology and Performances of Photovoltaic devices based on Thieno[3,4-c]pyrrole-4,6-dione-Based Donor-Acceptor Conjugated Polymers and CdSe Tetrapods

Abstract: We have prepared photovoltaic devices based on blend films of CdSe tetrapods and donor-acceptor conjugated polymer, PDTTTPD, comprising 2,5-di(thiophen-2-yl)thieno[3,2-b]thiophene and thieno[3,4-c]pyrrole-4,6-dione units. The AM1.5 power conversion efficiency of a photovoltaic device containing PDTTTPD/CdSe tetrapods (1:9. w:w) blend that has experienced thermal annealing at 130 °C for 20 min improved to 2.9% from 1.0% for a device comprising as-prepared PDTTTPD/CdSe tetrapod blend, an increase of three-fold. Synchrotron X-ray reflectivity measurements revealed that the thickness decreased and the average density increased relative to the as-prepared PDTTTPD/CdSe tetrapods blend film, after the removal of pyridine on the CdSe tetrapods' surface upon annealing. Transmission electron microscopy and atomic force microscopy studies revealed that the thermal annealing critically enhances the aggregation of CdSe tetrapods and induces denser morphologies, leading to a substantially increased charge transport, which enhances the power conversion efficiency of the device.

Introduction:

Solution-processing of bulk heterojunction (BHJ) photovoltaic devices that has been used successfully include polymer-polymer,^[1-4] polymer-C₆₀ derivatives,^[5-10] and polymer-nanocrystal blend^[11-17], which are an attractive area of investigation because many potential benefits, particularly for the rapid and economical preparation of flexible, large-area devices. The development of composite materials comprising a conjugated polymer as the hole acceptor and solution-processable inorganic semiconductor nanocrystal as the electron acceptor for use in BHJ photovoltaic systems has undergone rapid advances, becoming a particularly active area of investigation. For example, conjugated polymer/nanocrystal photovoltaic devices containing CdSe nanocrystals, one of the most investigated materials as the electron acceptor, have been fabricated in combination with poly(3-hexylthiophene) (P3HT)^[18-21], OC1C10 PPV,^[22-23] MEH-PPV,^[24] and alternating polyfluorene copolymer APFO-3^[25] as the hole acceptors, have exhibited an AM1.5G power conversion efficiencies (PCEs) in the range of 1.4-2.6%. Moreover, large improvements in PCEs have been obtained when combining CdSe tetrapods and Poly[2,6-(4,4-bis-(2-ethyl-hexyl)-4H-cyclopenta[2,1-b;3,4-b']-dithiophene)-alt-4,7-(2,1,3-benzo-thiadiazole)](PCPDTBT), leading to an AM1.5 PCE of 3.1%.^[26] Recently, It has been deeply studied that the shape of CdSe nanocrystals affects the device performance when blended with polymers.^[27] The device performance of the tetrapod-shaped nanocrystals (tetrapods) was better than that of nanorods and spherical nanocrystals, because of the tetrapods with a optimum arrangement for electron extraction.^[22]

In principle, BHJ photovoltaic devices should exhibit an excellent photovoltaic performance when comprising polymer/CdSe nanocrystals BHJ photovoltaic devices due to the high absorption coefficient and tunable bandgap of CdSe nanocrystals, however, the performances of the devices were smaller than polymer/fullerene BHJ photovoltaic devices in the past researches, owing to the complicated surface of nanocrystals.^[28] The surfaces of inorganic semiconductor nanocrystals typically possess long-chain and electrically insulating organic ligands, which must be shortened or removed for use in optoelectronic device applications.^[29-32] A major challenge of current research into inorganic semiconductor nanocrystals is to devise methods for ligand exchange or ligand removal to reduce the inter-nanocrystals spacing and, thereby, create more dense and conductive films.

Furthermore, in recent years, conjugated polymers containing alternating donor (D) and acceptor (A) units in their main^[33-34] or side^[35-36] chains have been applied widely in BHJ photovoltaic devices because of their readily tunable electronic properties. The electron-deficient thieno[3,4-c]pyrrole-4,6-dione (TPD) moiety exhibits a symmetric, rigidly fused, coplanar structure and strong electron-withdrawing properties, which make it a potential system for increasing intramolecular/intermolecular interactions, and lowering highest occupied molecular orbital (HOMO) energy levels when incorporated into polymeric backbones, resulting in enhanced values of Voc in BHJ solar cells.^[37-40]

In this study, we investigated the effects of the thermal annealing on the morphology and photovoltaic device performance of thin films comprising the CdSe tetrapods and donor-acceptor conjugated polymer, PDTTTPD, comprising 2,5-di(thiophen-2-yl)thieno[3,2-b]thiophene and thieno[3,4-c]pyrrole-4,6-dione units. We expect the removal of pyridine on the CdSe tetrapods'

surface after annealing will affect the packing density and nanoscale morphology^[41] of the active layer in the photovoltaic devices and the device performances. The optimum arrangement CdSe tetrapods in the active layer provide not only interfaces for the charge separation of photogenerated excitons but also percolation pathways for carrier transport to the respective electrodes, leading to improvement in devices' power conversion efficiency. We used attenuated total reflection Fourier transform infrared (ATR-FTIR) spectroscopy and synchrotron X-ray reflectivity (XRR) probe provide a deep understanding of the chemical structure, thickness and density of PDTTTPD/CdSe films. In addition, using transmission electron microscopy (TEM), and atomic force microscopy (AFM), the relationship between the nano-morphology and the device performance can be elucidated.

Results and Discussion:

Figure 1a shows the molecular structure of the donor–acceptor polymer PDTTTPD that contains alternating rigid, coplanar, electron-rich DTT units and rigid, electron-deficient TPD used in the photovoltaic device. The synthesis of the PDTTTPD polymers was described elsewhere.^[42] The PDTTTPD copolymer incorporating DTT and TPD units into the backbone would provide relatively low-lying HOMO energy levels, resulting in enhanced values of V_{oc} when used in photovoltaic applications. **Figure 1b** displays a TEM image of CdSe tetrapods used in the devices. The TEM image illustrated high yields of branched nanoparticles were synthesized and the tetrapod with a core and four arms can be observed clearly. Moreover, the tetrapods have arms with the average diameter of ~5 nm and with the length in a range of 25-50 nm.

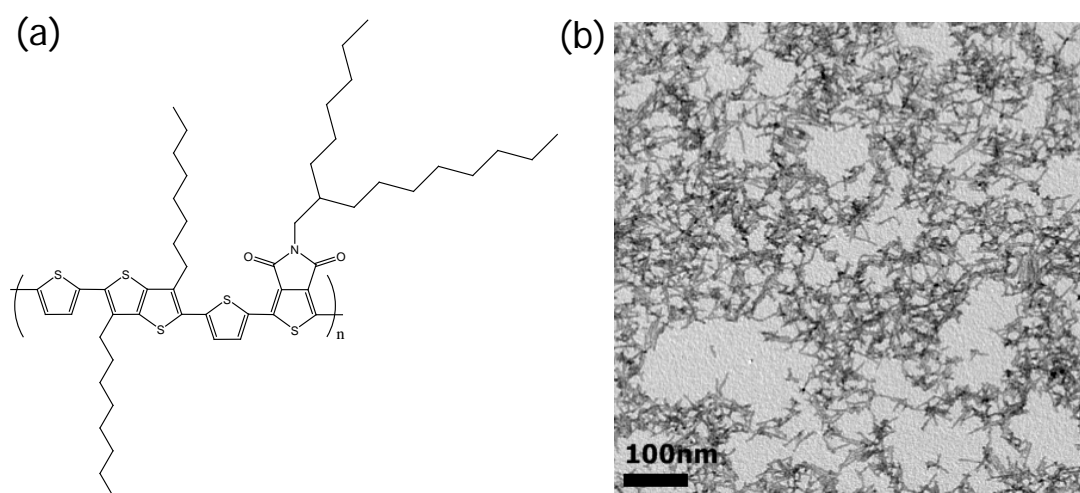


Figure 1. (a) Molecular structure of PDTTTPD. (b) TEM image of CdSe tetrapods. Scale bar, 100nm.

Figure 2a presents the optical absorption spectra of spin-coated films of pyridine treated CdSe tetrapods, pure PDTTTPD and PDTTTPD/CdSe (1:9, w/w) blend. The pyridine-treated CdSe tetrapods thin film, exhibits a first absorption peak at 630 nm and strong absorbance in the shorter wavelength region between 350 and 550 nm, complementing the inferior absorption from the polymers in this region. In the spectrum of PDTTTPD thin film, we assign the absorption maximum at 510 nm to intra-molecular charge transfer interactions between the **DTT** donor and **TPD** acceptor. The absorption signal of PDTTTPD is red-shifted by ca. 23 nm in thin film relative to that in solution, indicating that considerably strong intermolecular interactions and aggregation in the solid film, shown in **Figure 3**. In addition, we observed a vibronic shoulder at 620 nm in the spectrum, attributable to ordered molecular arrangement such as π - π stacking between the polymer backbones during the precipitation process. In the composite films, shows a superposition of respective absorption spectra of pure PDTTTPD and CdSe components, indicating that there is no electronic interaction between the PDTTTPD polymer and the CdSe tetrapods. The photovoltaic device, presented in **Figure 2b** shows the architecture of a fabricated device with a sandwich structure (ITO/PEDOT:PSS/PDTTTPD:CdSe tetrapods (1:9, w/w)/Al). The transparent and conducting ITO

layer and forms the bottom contact of the device. After PEDOT:PSS was coated, the PDTTTPD/CdSe tetrapods blend was spin-coated from a chloroform/pyridine/dichlorobenzene solution and then thermally annealed at 130°C for various lengths of time. Finally, a 100 nm thick Al film is used as the top contact and is deposited by evaporation either directly onto the active layer.

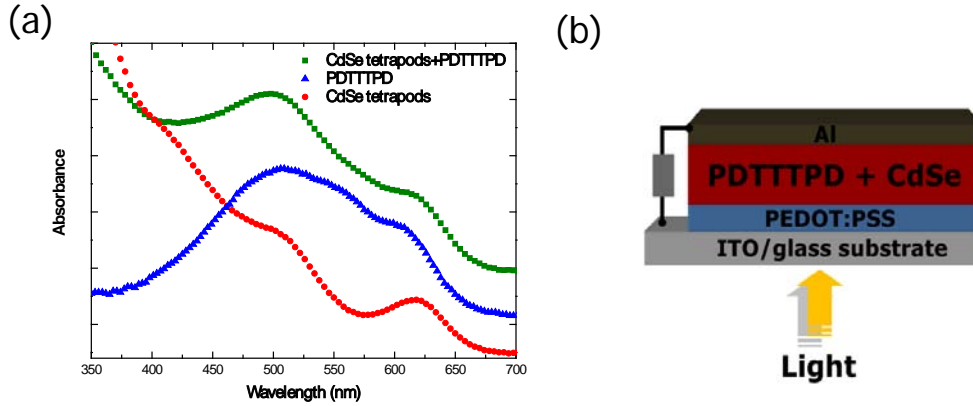


Figure 2. (a) Optical absorption spectra for spin-coated films of pure PDTTTPD (triangles), pure CdSe tetrapods (circles), and the PDTTTPD/CdSe tetrapods blend (squares). (b) Schematic structure of a PDTTTPD/ CdSe tetrapods photovoltaic device.

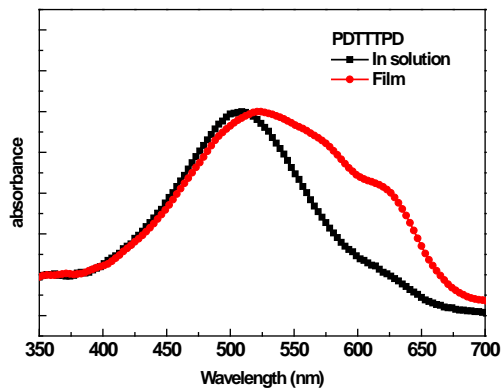


Figure 3. Optical absorption spectra of PDTTTPD were in CHCl_3 and as a solid film.

Figure 4a shows the current density–voltage characteristics of the photovoltaic devices that comprised PDTTTPD/CdSe (1:9, w:w) active layers with thermal annealing at 130°C for 10–30 min. All the devices incorporated a thin PEDOT:PSS hole transport layer to improve the photovoltaic performance and stability^[43] and measured under AM1.5G illumination (100 mW cm^{-2}) in a N_2 -filled glovebox. The thickness of the active layer in each of these devices was $130 \pm 20 \text{ nm}$, as measured using a profile-meter. **Table 1** lists the short-circuit current densities (J_{sc}), V_{oc} , fill factor (FF) and power conversion efficiencies of these heterojunction PDTTTPD-CdSe photovoltaic devices. The values of V_{oc} for these blend devices experienced annealing for different times were in the range of 0.88-0.89V, only slightly different. Due to the value of V_{oc} of a BHJ device is generally associated with the difference between the HOMO energy level of the polymer and the lowest unoccupied molecular orbital (LUMO) energy level of CdSe tetrapods,^[44] we suppose that the PDTTTPD/CdSe tetrapods blends exhibited these high values of V_{oc} because of the low-lying HOMO energy level of PDTTTPD. The values of J_{sc} and FF of the PDTTTPD/CdSe blend devices after annealing treatment

were significantly higher than that of the as-prepared blend device. For example, the value of J_{sc} of the blend device with thermal annealing at 130°C for 20min was approximately two times as large as that of the as-prepared blend device (7.26 vs. 3.16 mA/cm²). **Figure 5** presents the device characteristics of the blends that we subjected to annealing at temperatures of 110–140 °C. Among all of the devices we studied, the device containing PDDTTTPD/CdSe blend that was thermally treated at 130 °C for 20 min exhibited the highest power-conversion efficiency of 2.9 %, nearly three times as large as that of the as-prepared device, 1.0 %.

The inset of **Figure 4a** displays the energy band diagram for the various layers in the device, the energy level offset between the PDDTTTPD polymer and the CdSe tetrapods, indicate that the tetrapods act as electron acceptor and polymer as hole acceptor for the dissociation of photogenerated excitons. From the previous study,^[42] the HOMO and lowest unoccupied molecular orbital (LUMO) energy levels of PDDTTTPD were determined to be -5.5 and -3.0 eV, respectively. The presence of the TPD moiety provided the polymer with a low-lying HOMO energy level, indicating that the moiety is strongly electron-withdrawing; moreover, the HOMO energy level of PBTTPD (-5.5 eV) was located significantly below -5.2 eV, implying good stability against oxidization in air,^[39] a property that would enhance device stability.

We also measured the external quantum efficiencies (EQEs) of the devices with annealing treatment at 130 °C for different times. **Figure 4b** displays EQE curves of the devices containing active layer s of PDDTTTPD/CdSe (1:9, w:w); each device exhibited a broad EQE response from 300 to 700 nm. Moreover, the broad peaks observed in the region shorter than 450 nm, where PDDTTTPD has little absorption, clearly shows the evidence of the absorption due to the CdSe tetrapods, which effectively indicates CdSe and PCPDTBT response in the blend devices. Furthermore, in the range from 320 to 650 nm, the absolute EQEs of the device prepared from PDDTTTPD/CdSe tetrapods annealed at 130 °C for different times were much higher than that of the device containing the as-prepared blends. For example, the EQEs at 500nm for the devices containing PDDTTTPD/CdSe tetrapods that experience annealing at 130 °C for 20 min and comprising as-prepared were 53 and 23%, respectively—a two-fold increase for the former over the latter while at 640 nm, the corresponding values were 21 and 7%, respectively—almost a three-fold increase. The calculated values of J_{sc} can be obtained by integrating the EQE values with an AM 1.5G reference spectrum; the calculated values of 3.0, 6.2, 6.9, and 6.7 mA cm⁻² for the devices processed using annealed at 130 °C for 0, 10, 20, and 30min, respectively, are in reasonable agreement (within ±5% error) with the corresponding values of J_{sc} (3.1, 6.5, 7.2, and 6.9 mA cm⁻², respectively) obtained from the J - V measurements. We suspect that the improvement in the J_{sc} was resulted from the removal of the pyridine groups from the surface of CdSe tetrapods which would allow efficient charge generation and collection. Since the morphology change of the active layer thin film can also be an important contribution to the improvement in the device performance,^[13] we probe the chemical structure, density, thickness, and morphology of the PDDTTTPD/CdSe tetrapods films on the as-prepared device and the optimal device that has been annealed at 130 °C for 20 min.

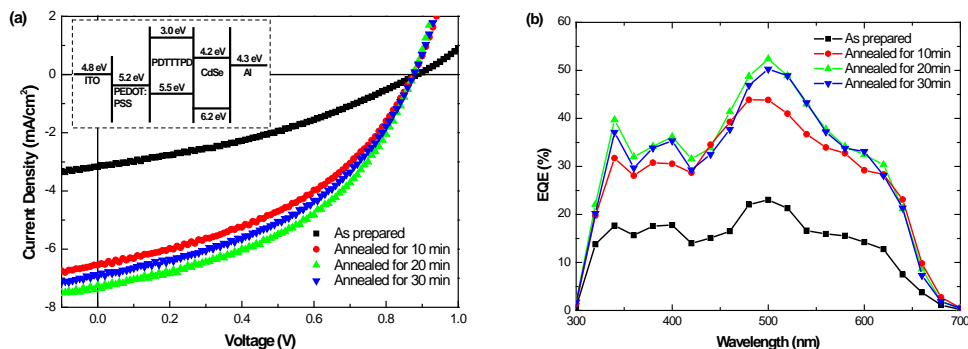


Figure 4. (a) Current–voltage characteristics and (b) EQE spectra of the PDDTTTPD/ CdSe tetrapods photovoltaic devices with thermal annealing at 130°C for various lengths of time. Inset shows the energy-level diagram for the PDDTTTPD/ CdSe tetrapods blend photovoltaic device. The devices were illuminated under AM1.5G conditions (100 mW cm⁻²).

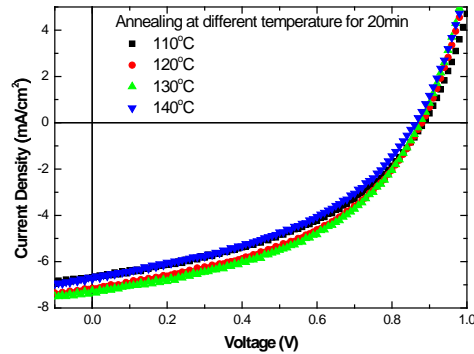


Figure 5. Current–voltage characteristics of the PDTTTPD/ CdSe tetrapods photovoltaic devices with thermal annealing at different temperature for 20min.

Figure 6 presents ATR-FTIR spectra of PDTTTPD/CdSe blend films that had experienced treatment with annealing and as prepared PDTTTPD/CdSe blend film; these spectra confirm the nature of the chemical species on the surfaces of the blend films. It is noted that all of the samples were containing 90 wt% CdSe tetrapods in PDTTTPD films, therefore, the signals were mostly contributed from the surface on the CdSe tetrapod. In the spectrum of the as-prepared blend film features the hill-like signals for C-C, C-N stretching at 1445 and 1600cm^{-1} , indicating the presence of pyridine bound to the CdSe.^[45] Moreover, the intensities of the both signals for C-C, C-N stretching at 1445 and 1600cm^{-1} in the spectrum of the annealed film were dramatically reduced relative to in the as prepared film, indicating that most of the pyridine ligands on the CdSe tetrapods had been removed, presumably because the pyridine was weak binding ligands that can be removed through thermal annealing.

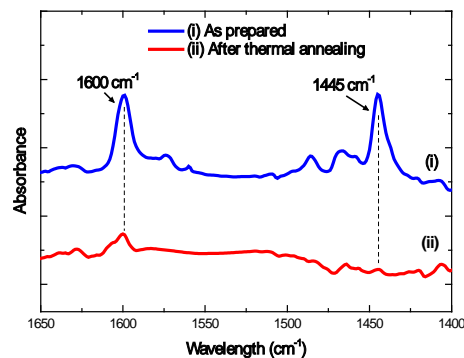


Figure 6. ATR- FTIR spectra of the PDTTTPD/ CdSe tetrapods blend films with and without thermal annealing (130°C , 20min).

Figure 7a presents synchrotron X-ray reflectivity (XRR) of the as-prepared and the annealed PDTTTPD/CdSe blend films that have been processed by spin-coating the solutions on ITO/PEDOT:PSS substrates. Our simulation of the specular reflectivity, allowing us to acquire the physical parameters of the multilayer, was based on the recursive formalism of Parratt,^[46] we then fitted the reflectivity data with the BedeREFS Mercury code^[47] to determine the physical parameters of the multilayer, including its thickness, and density. Moreover, the critical angle of total reflection, as indicated by the dashed line, increased substantially—implying increases in the average film density—after the film was thermal annealed at 130°C for 20 min. The fitted densities for as-prepared and annealed films were 2.9 , and 3.2 g cm^{-3} , respectively. Annealing treatment of the

PDTTTPD/CdSe tetrapods film caused the thickness of the film to decrease to 135 from 150 nm, with an associated increase in the film density. Therefore, the removal of pyridine ligands on the CdSe reduce the inter-particle distances, which in turn leads to higher CdSe tetrapods' packing densities and therefore provides better conductivities in the active layer. In addition, we also proceeded to determine the crystallinity of PDTTTPD in films with and without annealing using grazing incidence X-ray diffraction (GIXRD) measurement, shown in **Figure 7b**; however, there was no peak appeared in both XRD curves. Because of the high percentage of three-dimension CdSe nanostructures (90 wt%) loading in the blend film can destroy the ordering of the PDTTTPD polymer chains.

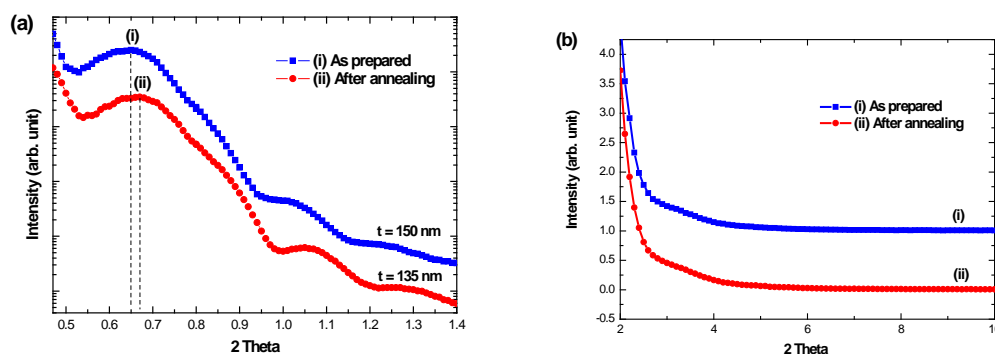


Figure 7. (a) Synchrotron X-ray reflectance (XRR) and (b) grazing incidence X-ray diffraction (GIXRD) for structures incorporating PDTTTPD/ CdSe tetrapods blend layers with and without thermal annealing (130°C, 20min), prepared onto ITO/PEDOT:PSS substrates (log-normal scale).

Figure 8 presents TEM images of the blend films used to make the device, containing 90 wt% CdSe tetrapods in the PDTTTPD with and without thermal annealing. The bright and dark regions correspond to PDTTTPD- and CdSe tetrapods-rich domains, respectively, because the differences in the electron scattering densities of CdSe (5.6 g cm^{-3}) and polymers (1.1 g cm^{-3}) are quite large. **Figure 8a** displays that CdSe tetrapods were dispersed rather uniformly in the blended film without annealing. However, Figure 6b clearly shows that the degree of aggregation in CdSe tetrapods have increases substantially after thermal annealing, as the result of the removal of organic surfactants on the CdSe surface. Furthermore, the PDTTTPD-rich domain in **Figure 8b** become larger than that in **Figure 8a**, because of that distributed around CdSe aggregates was clearly present in the expanded view of the annealed blend film. Consequently, annealing is seen to aid both in the removal of interfacial pyridine and bringing tetrapods closer together. This aggregation of neighboring tetrapods is likely to improve electron transport between tetrapods, which occurs through thermal annealing treatment.

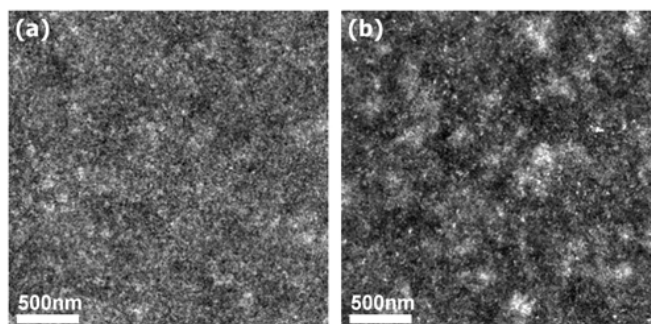


Figure 8. TEM images of the PDTTTPD/ CdSe tetrapods blend films (a) without and (b) with thermal annealing (130°C, 20min). Scale bar, 500nm.

Lastly, we also performed the studies of morphology of the PDTTTPD/CdSe tetrapods blend films

by using atomic force microscopy (AFM) in the tapping-mode, as it is often possible to identify local differences in the composition of the film by comparing the topography and phase image.^[13] **Figure 9a-b** show the AFM topography images of the blend films, indicated that the blend film with annealing becomes rougher than that without annealing. Moreover, the relative surface roughnesses of the films without and with annealing treatment determined from AFM were 6.8 and 9.5 nm, respectively. **Figure 9c-d** displays the corresponding AFM phase images demonstrate that the surface roughness relates to phase domains. The PDTTTPD polymer grain features are clearly evident in the phase contrast images of the blend films, due to that there appears to be little room for polymer to fully penetrate the tetrapods.^[12] Moreover, the minor aggregation of the CdSe tetrapods would decrease the space of PDTTTPD inside the individual tetrapods, resulting in the PDTTTPD polymer grain size in the AFM phase image was slightly increased after thermal annealing. Such optimum aggregation could significantly influence the physical interactions between the tetrapods and the polymer chains and improve the charge separation and transport through the blended film.^[28]

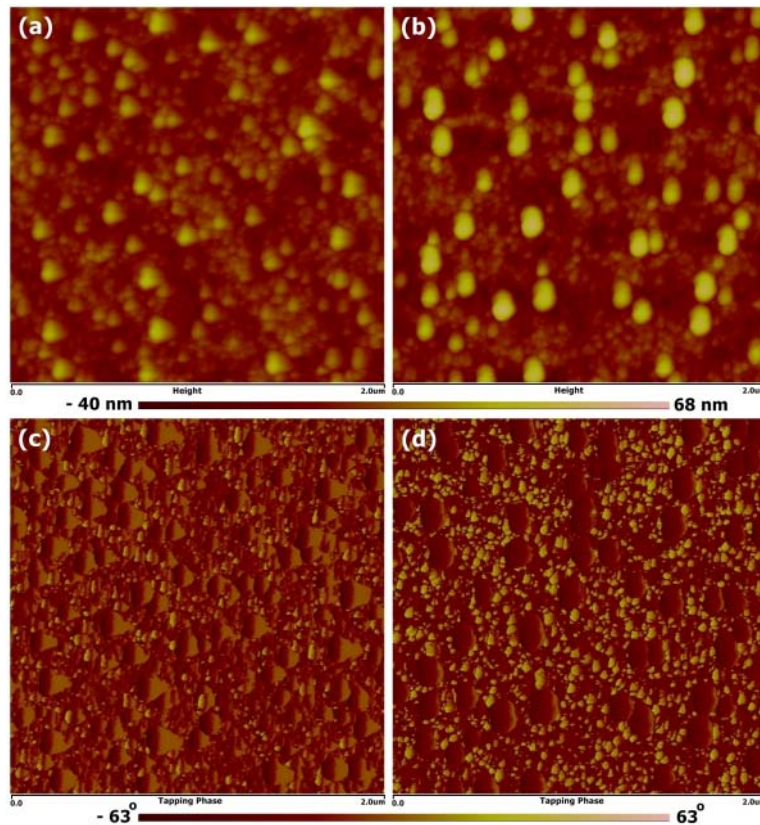


Figure 9. Tapping-mode topographic AFM images of the (a) as-prepared and (b) thermal annealed (130°C, 20min) PDTTTPD/ CdSe tetrapods blended films. The corresponding AFM phase images of films were (c) as-prepared and (d) annealed, respectively. The image size is 2 μm \times 2 μm .

Conclusion

In conclusion, we have demonstrated bulk-heterojunction photovoltaic devices based on PDTTTPD and CdSe tetrapods and optimized the power conversion of the devices with annealing treatments. Particularly, annealing PDTTTPD/ CdSe tetrapods (1:9, w:w) blend devices at 130 °C for 20min led to highly enhanced AM1.5 PCEs relative to those of blend devices without annealing treatment, with an enhancement factor of three-fold. This enhancement is owing to a sharp increase in the short current density of the device that contains a more dense active layer and aggregated CdSe tetrapods after thermal annealing, resulting from much less pyridine ligands on CdSe tetrapods. Therefore, the annealing process plays an important role in the improvement of the device performance and morphology.

Experiment:

Materials. PDTTTPD ($M_n = \text{ca. } 9,200 \text{ g mol}^{-1}$) was synthesized using a previously reported method^[42] and dissolved in 1,2-dichlorobenzene for device fabrication. 1,2-Dichlorobenzene used to dissolve PDTTTPD was a better solvent for the polymer than was chloroform, chlorobenzene, and trichlorobenzene. Moreover, CdSe tetrapods used for the photovoltaic devices were synthesized with the standard Schlenk line according to a previously reported method.^[22] Typically, 0.173 g of cadmium oxide, 0.535 g of octylphosphonic acid, and 1.293 g of tri-*n*-octylphosphine oxide were mixed in a three-neck flask and heated at 300 °C under vigorous stirring and continuous Ar flow for 15 min to obtain a colorless, clear solution. The mixture was cooled to room temperature and then stored in a nitrogen glove box as a cadmium precursor. After 2 days, the cadmium precursor was heated to 300°C and then the refrigerated solution containing 0.213g of Se, 0.635g of tributylphosphine, and 0.15 mL toluene was quickly injected into this hot solution. The temperature of the reaction solution was maintained at 250 °C for the growth of CdSe tetrapods. After allowing the reaction to proceed for 50min, the mixture was quenched by adding 4mL toluene. The tetrapods were isolated from the growth mixture through repeated precipitations with methanol prior to being dispersed in toluene. For ligand exchange, the as-synthesized CdSe tetrapods were redispersed in anhydrous pyridine and stirred continuously at 110°C overnight in a N₂-filled glove box to remove the original ligands. Finally, the resultant QDs were precipitated with anhydrous hexane and redispersed in anhydrous pyridine/chloroform (1:9) for device fabrication. All other reagents were used as received from commercial sources, without further purification.

Material Characterization. Attenuated total reflection Fourier transform infrared (ATR-FTIR) spectra were recorded at room temperature using a Perkin–Elmer Spectrum100 instrument and optical absorption data were acquired with a Hitachi U-4100 spectrophotometer equipped with an integrating sphere. Synchrotron X-ray reflectivity (XRR) analyses were performed at the wiggler beamline BL-17B1 using an eight-circle diffractometer at the National Synchrotron Radiation Research Center (NSRRC), Hsinchu, Taiwan; the photon energy was 8 keV and the flux was estimated to be 1011 photons s⁻¹. The use of two pairs of slits between the sample and the detector provided a typical wave-vector resolution of ca. 0.001 nm⁻¹ in the vertical scattering plane. TEM images were obtained using an FEI Tecnai Spirit TWIN apparatus operated at 120 keV. For TEM analysis, the devices were first placed into water and, after the active layers had floated to the surface, they were transferred to the TEM grid. The devices' morphologies were recorded under ambient conditions using an atomic force microscope operated in the tapping mode and a Veeco Innova instrument.

Device Fabrication and Characterization. We investigated the current density–voltage (J – V) characteristics of the devices with a sandwich structure (ITO/PEDOT:PSS/PDTTTPD:CdSe tetrapods (1:9, w/w)/Al). The patterned ITO on the glass substrate ($5 \Omega \text{ sq.}^{-1}$, Merck) was cleaned through sequential ultrasonic treatment with detergent, methanol, acetone, and isopropanol and then dried under a flow of N₂. PEDOT:PSS (Baytron P VP AI 4083) was then spin-coated on the ultraviolet ozone-treated ITO and annealed at 150 °C for 1 hour before transferring to a nitrogen glovebox. Afterwards, the PDTTTPD/CdSe tetrapods blend solution (28mg mL⁻¹) was spin-coated (900 rpm, 60 s) on top of the PEDOT:PSS layers. The thickness of the active layers were typically 130± 20 nm thick measured using a Veeco Dektak 150 surface profilometer. Subsequently, the active layers of our devices were dried slowly in a covered dish for 1h and then thermally annealed at 130 °C for 20 min prior to electrode deposition. Using a base pressure at ca. 10⁻⁷ torr, 100-nm Al top electrodes were deposited onto all of the samples by thermal evaporation through a shadow mask. Four devices were fabricated on each substrate, each with an active area of 0.04 cm².

The J – V characteristics of the devices were measured by illuminating these devices through a mask that fits the electrode crossing area under simulated AM1.5G irradiation (100 mW cm⁻²) using a Xe lamp-based Newport 66902 150-W solar simulator equipped with a Keithley 2400 source measurement unit. The spectral mismatch factor was calculated by comparing the solar simulator spectrum with the AM 1.5 G (ASTM G173) spectrum. EQEs were measured using an SR150 (Optosolar GmbH, Germany) spectral response measurement setup.

Reference

- [1] M. Granström, K. Petritsch, A. C. Arias, A. Lux, M. R. Andersson, and R. H. Friend, *Nature*, 1998, 395, 257.
- [2] T. Kietzke, H. H. Hörhold, and D. Neher, *Chem. Mater.*, 2005, 17, 6532.
- [3] H. J. Snaith, N. C. Greenham, and R. H. Friend, *Adv. Mater.*, 2004, 16, 1640.
- [4] M. M. Koetse, J. Sweelssen, K. T. Hoekerd, H. F. M. Schoo, S. C. Veenstra, J. M. Kroon, X. Yang, and J. Loos, *Appl. Phys. Lett.*, 2006, 88, 083504.
- [5] H. Y. Chen, J. Hou, S. Zhang, Y. Liang, G. Yang, Y. Yang, L. Yu, Y. Wu, and G. Li, *Nature Photonics*, 2009, 3, 649–653.
- [6] W. Ma, C. Y. ang, A. J. Heeger, *Adv. Mater.*, 2007, 19, 1387–1390.
- [7] B. Kippelen, and J. L. Bredas, *Energy Environ. Sci.*, 2009, 2, 251–261.
- [8] S. B. Darling, *Energy Environ. Sci.*, 2009, 2, 1266–1273.
- [9] F. Huang, K. S. Chen, H. L. Yip, S. K. Hau, O. Acton, Y. Zhang, J. Luo, and A. K. Y. Jen, *J. Am. Chem. Soc.*, 2009, 131, 13886.
- [10] T. Ameri, G. Dennler, C. Lungenschmied, and C. J. Brabec, *Energy Environ. Sci.*, 2009, 2, 347–363.
- [11] K. M. Noone, and D. S. Ginger, *ACS Nano*, 2009, 3, 261–265.
- [12] I. Gur, N. A. Fromer, C. P. Chen, A. G. Kanaras and A. P. Alivisatos, *Nano Lett.*, 2007, 7, 409–414.
- [13] W. U. Huynh, J. J. Dittmer, W. C. Libby, G. L. Whiting and A. P. Alivisatos, *Adv. Funct. Mater.*, 2003, 13, 73–79.
- [14] Y. Zhou, M. Eck, and M. Krüeger, *Energy Environ. Sci.*, 2010, 3, 1851–1864.
- [15] D. V. Talapin, J. S. Lee, M. V. Kovalenko and E. V. Shevchenko, *Chem. Rev.*, 2010, 110, 389–458.
- [16] S. A. McDonald, G. Konstantatos, S. Zhang, P. W. Cyr, E. J. D. Klem, L. Levina, and E. H. Sargent, *Nat. Mater.*, 2005, 4, 138–142.
- [17] D. H. Cui, J. Xu, T. Zhu, G. Paradee, S. Ashok, and M. Gerhold, *Appl. Phys. Lett.*, 2006, 88, 183111.
- [18] B. Q. Sun, and N. C. Greenham, *Phys. Chem. Chem. Phys.*, 2006, 8, 3557–3560.
- [19] Y. F. Zhou, F. S. Riehle, Y. Yuan, H. F. Schleiermacher, M. Niggemann, G. A. Urban, and M. Krüeger, *Appl. Phys. Lett.*, 2010, 96, 013304.
- [20] J. S. Liu, T. Tanaka, K. Sivula, A. P. Alivisatos, and J. M. J. Fréchet, *J. Am. Chem. Soc.*, 2004, 126, 6550–6551.
- [21] J. D. Olson, G. P. Gray, and S. A. Carter, *Sol. Energy Mater. Sol. Cells*, 2009, 93, 519–523.
- [22] B. Q. Sun, E. Marx, and N. C. Greenham, *Nano Lett.*, 2003, 3, 961–963.
- [23] B. Q. Sun, H. J. Snaith, A. S. Dhoot, S. Westenhoff, and N. C. Greenham, *J. Appl. Phys.*, 2005, 97, 014914.
- [24] Y. Zhou, Y. C. Li, H. Z. Zhong, J. H. Hou, Y. Q. Ding, C. H. Yang, and Y. F. Li, *Nanotechnology*, 2006, 17, 4041–4047.
- [25] P. Wang, A. Abrusci, H. M. P. Wong, M. Svensson, M. R. Andersson, and N. C. Greenham, *Nano Lett.*, 2006, 6, 1789–1793.
- [26] S. Dayal, N. Kopidakis, D. C. Olson, D. S. Ginley, and G. Rumbles, *Nano Lett.*, 2010, 10, 239–242.
- [27] S. Dayal, M. O. Reese, A. J. Ferguson, D. S. Ginley, G. Rumbles, and N. Kopidakis, *Adv. Funct. Mater.*, 2010, 20, 2629–2635.
- [28] Y. Wu, and G. Zhang, *Nano Lett.*, 2010, 10, 1628–1631.
- [29] C. Y. Kuo, M. S. Su, C. S. Ku, S. M. Wang, H. Y. Lee, and K. H. Wei, *Journal of Materials Chemistry*, 2011, DOI: 10.1039/c0jm04417b.
- [30] D. V. Talapin, and C. B. Murray, *Science*, 2005, 310, 86–89.
- [31] J. M. Luther, M. Law, Q. Song, C. L. Perkins, M. C. Beard, and A. J. Nozik, *ACS Nano*, 2008, 2, 271–280.
- [32] R. Debnath, J. Tang, D. A. Barkhouse, X. Wang, A. G. Pattantyus-Abraham, L. Brzozowski, L. Levina, and E. H. Sargent, *J. Am. Chem. Soc.*, 2010, 132, 5952–5953.
- [33] B. Kim, B. Ma, V. R. Donuru, H. Liu and J. M. J. Fréchet, *Chem. Commun.*, 2010, 46, 4148.
- [34] J. Ding, N. Song and Z. Li, *Chem. Commun.*, 2010, 46, 8668.
- [35] Y. T. Chang, S. L. Hsu, M. H. Su and K. H. Wei, *Adv. Mater.*, 2009, 21, 2093.
- [36] F. Huang, K. S. Chen, H. L. Yip, S. K. Hau, O. Acton, Y. Zhang, J. Luo and A. K. Y. Jen, *J. Am. Chem. Soc.*, 2009, 131, 13886.

- [37] C. Piliago, T. W. Holcombe, J. D. Douglas, C. H. Woo, P. M. Beaujuge and J. M. J. Fréchet, *J. Am. Chem. Soc.*, 2010, 132, 7595.
- [38] A. Najari, S. Beaupré, P. Berrouard, Y. Zou, J. R. Pouliot, C. L Pérusse and M. Leclerc, *Adv. Funct. Mater.*, 2010, DOI: 10.1002/adfm.201001771.
- [39] Y. Zou, A. Najari, P. Berrouard, S. Beaupré, B. R. Aïch, Y. Tao and M. Leclerc, *J. Am. Chem. Soc.*, 2010, 132, 5330.
- [40] M. C. Yuan, M. Y. Chiu, S. P. Liu, C. M. Chen and K. H. Wei, *Macromolecules*, 2010, 43, 6936.
- [41] Y. Kim, S. Cook, S. M. Tuladhar, S. A. Choulis, J. Nelson, J. R. Durrant, D. D. C. Bradley, M. Giles, I. McCulloch, C. S. Ha, M. Ree, *Nat. Mater.* 2006, 5, 197–203.
- [42] G. Y. Chen, Y. H. Cheng, Y. J. Chou, M. H. Su, C. M. Chen, and K. H. Wei, *Chem. Commun.*, 2011, DOI:10.1039/C1CC10585J.
- [43] C. Y. Kuo, M. S. Su, Y. C. Hsu, H. N. Lin, and K. H. Wei, *Adv. Funct. Mater.*, 2010, 20, 3555–3560.
- [44] M. C. Scharber, D. Mühlbacher, M. Koppe, P. Denk, C. Waldauf, A. J. Heeger, C. J. Brabec, *Adv. Mater.* 2006, 18, 789–794.
- [45] B. S. Kim, L. Avila, L. E. Brus, and I. P. Herman, *Appl. Phys. Lett.*, 2000, 76, 3715-3717.
- [46] L. G. Parratt, *Phys. Rev.*, 1954, 95, 359–369.
- [47] D. K. Bowen, and B. K. Tanner, *Nanotechnology*, 1993, 4, 175–182.

List of Publications:

1. Chih-Yin Kuo, Ming-Shin Su, Yu-Chien Hsu, Hui-Ni Lin, and Kung-Hwa Wei*, *Advanced Functional Materials*, **2010**, 20, 3555-3560. (IF 6.99)
2. Chih-Yin Kuo, Ming-Shin Su, Ching-Shun Ku, Shu-Min Wang, Hsin-Yi Lee, and Kung-Hwa Wei*, *J. Mater. Chem.* **2010**, DOI: 10.1039/c0jm04417b. (IF 4.795)
3. Chih-Yin Kuo, Ming-Shin Su, Ching-Shun Ku, Guan-Yu Chen, Hsin-Yi Lee, and Kung-Hwa Wei*, *Energy Environ. Sci.* **2011**, submitted. (IF 8.5)